



2010 SEA-CSSJ-CMS TRILATERAL MEETING ON CLAYS

FIELD TRIP GUIDE AND ABSTRACTS OF THE SEPIOLITE SYMPOSIUM

June 7th, 2010
Madrid-Seville, Spain

Organized by:
Clay Minerals Society (CMS)
Clay Science Society of Japan (CSSJ)
Spanish Clay Society (SEA)



2010 SEA-CSSJ-CMS TRILATERAL MEETING ON CLAYS

FIELD TRIP GUIDE AND ABSTRACTS OF THE SEPIOLITE SYMPOSIUM

June 7th, 2010
Madrid-Seville, Spain

Organized by:
Clay Minerals Society (CMS)
Clay Science Society of Japan (CSSJ)
Spanish Clay Society (SEA)

Depósito Legal:
ISBN: 978-84-693-2652-7

Editors: J. Cuevas, J. F. Barrenechea, E. García-Romero,
S. Leguey, and J. Luque

Cover design: Felipe Bruna

SPONSORS



Spanish Ministry of Science & Innovation



Andalusian Government (Junta de Andalucía:
Instituto de Investigación y Formación Agraria y
Pesquera de Andalucía, IFAPA, Consejería de
Agricultura y Pesca, CAP y Consejería de
Economía, Innovación y Ciencia, CEIC)



Consejo Superior de Investigaciones Científicas
(CSIC)



Universidad de Sevilla



Bruker



IESMAT



BEL JAPAN, INC.

LOCAL COMMITTEE FOR SEPIOLITE SYMPOSIUM

Jaime Cuevas (Universidad Autónoma de Madrid)
José F. Barrenechea (Universidad Complutense de Madrid)
Emilia García Romero (Universidad Complutense de Madrid)
Santiago Leguey (Universidad Autónoma de Madrid)
Javier Luque (Universidad Complutense de Madrid)

Departamento de Cristalografía y Mineralogía



Departamento de Geología y Geoquímica



Preface

This field trip is organized within the Trilateral Clay Meeting held in Spain by the Clay Minerals Society (CMS), the Clay Science Society of Japan (CSSJ) and the Spanish Clay Society (SEA). This book contains the itinerary of the field trip and a summary of the geology of the Madrid Basin. The abstracts of the invited lectures for the sepiolite Symposium are also included.

The Madrid Basin is well-known by the occurrence of huge concentrations of Mg-rich clays. It hosts the world's largest sepiolite deposit. The Madrid Basin is an intra-plate basin, which originated during the late activation of Hercynian faults from the end of the Cretaceous to the Pliocene. Sepiolite is associated with other magnesium-rich clays (saponite, stevensite, and palygorskite), calcretes, and silcretes, formed within a lacustrine sedimentary environment. A short but significant visit to mining works, some few kilometres southward from Madrid, will take place. The visit will include geological observations at the sepiolite quarries in Vicálvaro (Madrid) and Cabañas de la Sagra (Toledo).

We would like to acknowledge Prof. E. Galán, for his generous contribution to the organization of the Symposium. Thanks also to Javier Berrio and Antonio Álvarez (TOLSA) and Daniel Tejela (Süd Chemie) for their helpful support during the preparation and development of the field trip. Finally we would like to acknowledge national and international sponsors for financial support to the three Societies that have made possible this Symposium.

LOCAL COMMITTEE FOR SEPIOLITE SYMPOSIUM

SUMMARY

Presentation	2
1. Geological Setting	3
2. Madrid Basin	5
2.1. Northern Area	9
The Vicálvaro-Barajas Area	9
2.2. Southern Area	16
Green Clay Unit	16
Fine-grained sands with sepiolite, chert and carbonate Unit	21
3. Mineralogy of Magnesium Clays	23
Bentonite Deposits	23
Pink Clays	25
Sepiolite Deposits	29
4. References	33
FIELD TRIP STOPS	39
ABSTRACTS OF SYMPOSIUM LECTURES	45

FIELD TRIP

PRESERNTATION

The trip begins in the Vicálvaro sepiolite quarry near Madrid (Figure 1), then continuing to Cabañas de la Sagra (Toledo), approximately 70 km southwards, near Toledo.

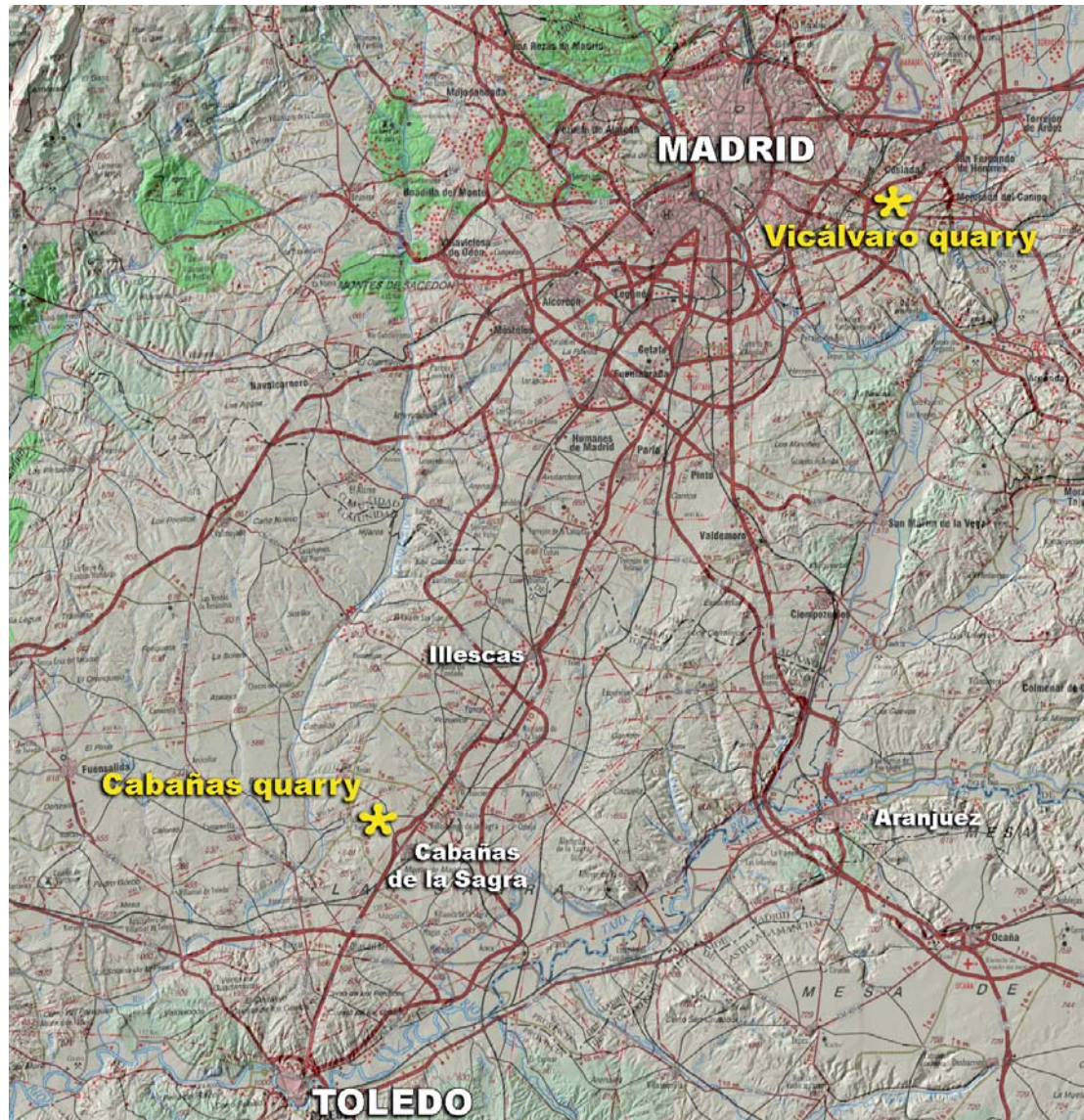


Figure 1. Location of the visited sepiolite quarries.

GEOLOGICAL SETTING

The Tajo Basin is located in the central part of the Iberian Peninsula (Fig. 2). It is a Tertiary basin developed during the Alpine orogeny, triangular in shape, and covering about 20000 km². It was originated by the movements of the African plate relative to the Iberian Massif. The basin is limited by mountain ranges which, in turn, were the source areas for the sediments filling the basin: the Central System, formed by granites and metamorphic rocks of Paleozoic age, to the north; the Iberian Range, mainly composed of carbonate and evaporite Mesozoic rocks, to the east; and the Toledo Mountains, also formed by granitic and high-grade metamorphic rocks, to the south (Fig. 2). The Tertiary infill of the basin has very variable thicknesses as a consequence of the differential movements of the basement during its formation. The maximum thickness, close to the Central System, is about 3500 m.

The Tajo Basin can be divided into two sub-basins: the Madrid Basin, to the west, and the Loranca Basin (also called Intermediate Depression). Both sub-basins are separated by the Altomira Range, which began to be developed at the end of the Paleogene (Megias et al., 1983; Ordoñez et al., 1991; Calvo et al., 1995). The Loranca Basin has been interpreted as a piggy-back basin, whereas the Madrid Basin is an intracratonic basin (Alonso-Zarza et al., 2004). Both sub-basins have scattered outcrops of Paleogene detrital sediments spatially distributed close to their margins, but most of the sedimentary infill corresponds to Miocene materials.

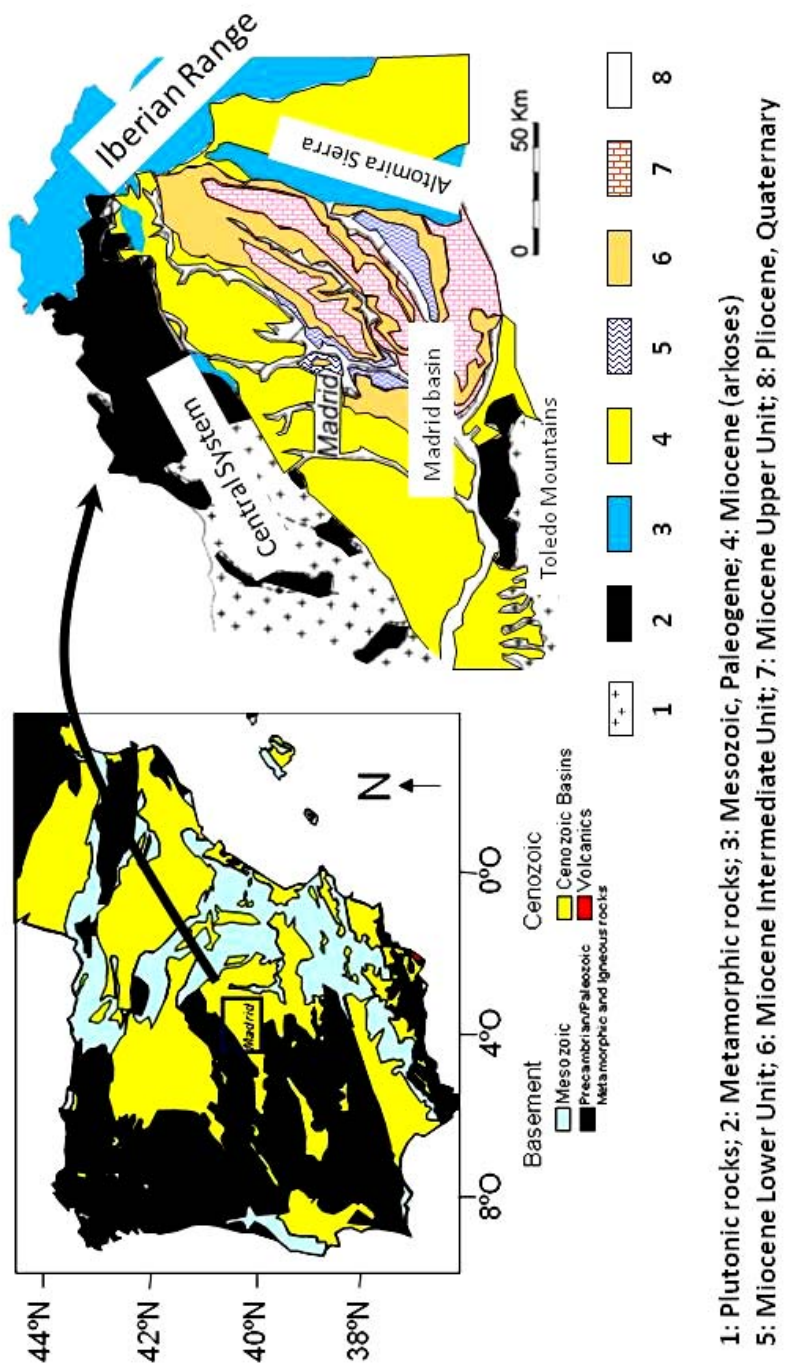


Figure 2. Cenozoic basins in the Iberian Peninsula, after Alonso-Zarza et al. (2004).

2. MADRID BASIN

The Miocene sediments of the Madrid basin have been divided into three lithostratigraphic units from bottom to top: Lower Unit, Intermediate Unit, and Upper Unit (Martín Escorza, 1976; Junco and Calvo, 1983; Megías et al., 1983; Portero and Aznar, 1984; Torres et al., 1984; Alberdi et al., 1985; Calvo et al., 1984, 1989; Ordoñez et al., 1991). The main features of these Units are outlined below and comprehensive descriptions can be found in Junco and Calvo (1983), Gibbons and Moreno (2002) and Alonso-Zarza et al. (2004).

Lower Unit

The sediments of this Unit overlie along an erosive discordance the Paleogene materials of the margins of the basin, but they lie conformably over the Paleogene sediments in the central parts of the basin (Alonso-Zarza et al., 1993). The age of this Unit is Ramblian to Lower Aragonian (Fig. 3), and its thickness varies from 600 to 1000 m.

The Lower Unit displays a concentric pattern of facies distribution, as a result of the distribution of hydrologically closed lacustrine systems during the Lower to Middle Miocene. Detrital facies close to the margins of the basin consist of detrital sediments corresponding to alluvial fan systems. These sediments are predominantly arkoses to the NW and S, and litharenites to the NE and E. Transitional facies deposited in mud flat environments have been recognized between the detrital and lacustrine sediments. These transitional facies mainly correspond to red clays with interbedded anhydrite nodules. Lacustrine sediments in the central part of the basin mostly correspond to evaporites, in which a complex mineral association including sulphates (anhydrite, thenardite, glauberite, and polyhalite), carbonates (dolomite and magnesite), and chlorides (halite) is recognized. These minerals are the result of the recycling of the Mesozoic and Paleogene evaporites. Ordóñez et al. (1991) related the alternation of carbonate and anhydrite deposits in the lower

part of the lacustrine sequence to seasonal variations, being anhydrite formed during dry seasons while carbonate formation would be associated with dilution of the brines by fresh waters during wet seasons. The upper part of the lacustrine sediments contains thenardite, formed in shallow seasonal endorheic ponds, with pH values close to neutral (García del Cura et al., 1986). Na-sulphates are mined from these lacustrine sediments.

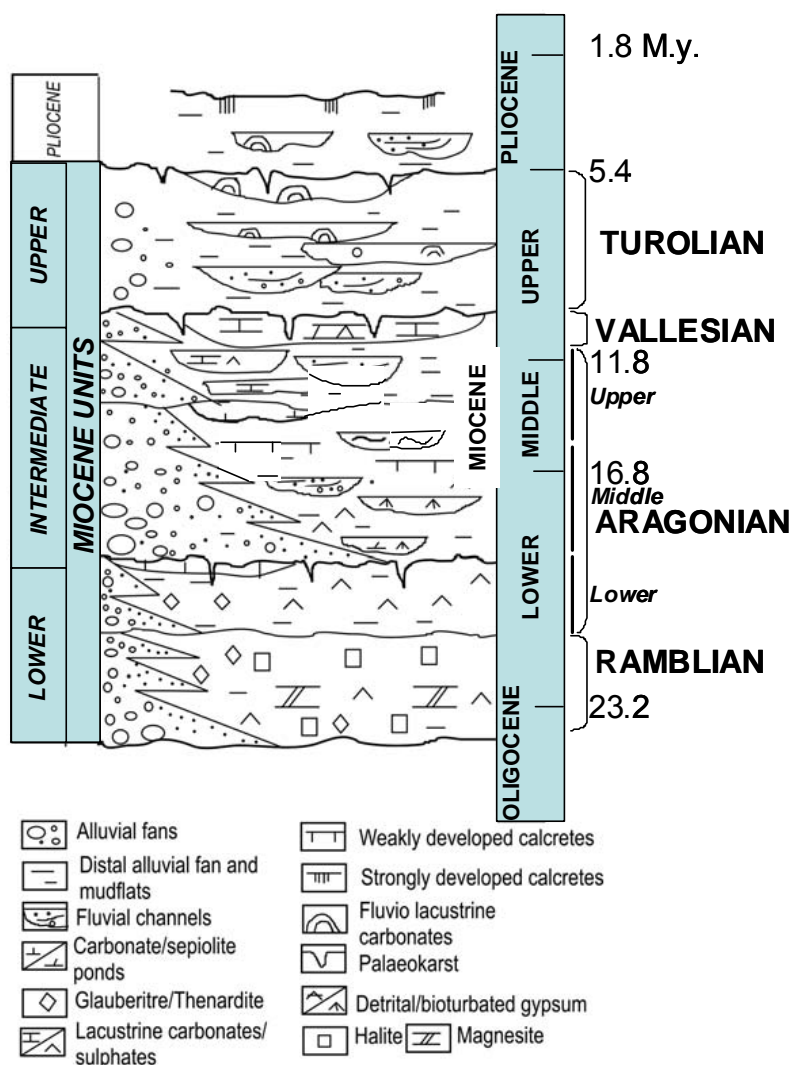


Figure 3. Stratigraphy of the Madrid Basin, showing the main Neogene units. From Bustillo and Alonso-Zarza (2007)

Intermediate Unit

The sediments of this Unit are Middle Aragonian to Vallesian in age, and also display a concentric pattern of facies distribution. They lie in disconformity over the Lower Unit and their thickness range from 50 to 200 m, thus pointing to a low sedimentation rate. The Intermediate Unit, as a whole, shows a clear trend to the diminution of the alluvial deposits leading to a greater development of lacustrine facies. Alluvial deposits form a discontinuous band (from a few hundreds of meters to 30 km wide) along the margins of the basin. The lithology and morphology of the source areas influenced the features of these depositional systems. Thus, in the northern and southern margins of the basin, arkose sands dominate, gradually passing to carbonate paleosols and clays in the distal facies of the alluvial fans and in the lacustrine systems. These clayey facies include the Mg-rich clay deposits (Mg-rich bentonite and sepiolite). Lacustrine sediments comprise gypsum (in the southern and eastern parts of the basin) and dolomite rocks developed under a shallow water environment with moderate salinity. In the northern part of the basin (Paracuellos del Jarama and Cerro del Telégrafo), associated with the fluvial-lacustrine facies transition, greenish clays (saponite) and sepiolite-chert layers have been reported (Bustillo and Alonso-Zarza, 2007). These saponitic clays also appear in the southern part of the basin as inselbergs (Cerros del Águila y del Monte) (Galán et al., 1986; Pozo et al., 1991; Cuevas et al., 1993; De Santiago et al., 1998).

Up to seven lacustrine events, in which sepiolite was formed, have been recognized, with vertical migration from NE to SW (Fig. 4). Maximum thickness of individual sepiolite levels is up to 35 m. This makes the world's largest sepiolite deposit with estimated reserves greater than 100 million tonnes.

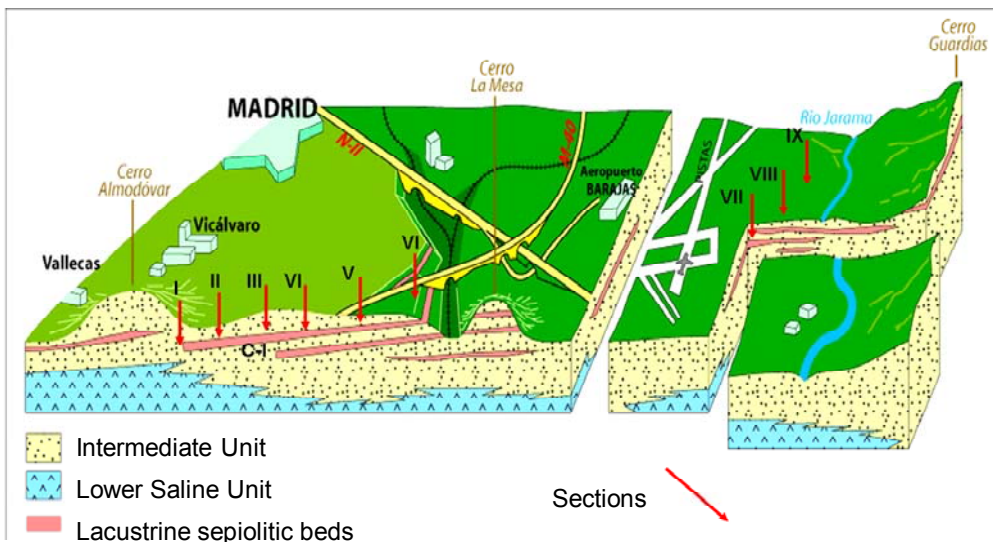


Figure 4. Lacustrine events with sepiolite at the NE of the Madrid Basin.

Upper Unit

This Unit, Vallesian to Turolian in age, does not show the above mentioned concentric facies distribution pattern. Maximum thickness is 50 m, and it lies along an erosive discordance over the Intermediate Unit. The base of the Upper Unit corresponds to detrital sediments (arkoses and litharenites) deposited in a fluvial system. To the top, carbonate rocks, mainly tuffs and micrites, dominate. These sediments were deposited in a fresh water fluvio-lacustrine system (Wright et al., 1997).

2.1. NORTHERN AREA

The Vicálvaro-Barajas area

At least seven layers (≥ 1 m thick) of lacustrine sedimentary rocks containing sepiolite can be recognized to the East of Madrid, in the Vicálvaro-Barajas area (Leguey et al., 1995). Three of these layers occur near Barajas at 520-560 m topographic level, with an average thickness of 2.5 m. In the Vicálvaro area, these layers are located in higher topographic positions (620-646 m). The layers are thicker than in Barajas, and sometimes reach up to 7 m, with a virtual pure sepiolite composition. The lacustrine episodes are progressively younger as we go from the NE to the SW, and result in elliptic-shaped deposits (2-5 Km long and 0.5-1 Km wide). According to Portero and Aznar (1984) the location of these lakes was controlled by the regional system of conjugated fractures (N45E and N120E).

The Vicálvaro sepiolite deposit (Fig. 5) is the most important one mined currently worldwide. It covers a 7.5 km^2 area elongated in NW-SE direction (5 km long and 1.5 km wide), with a maximum thickness of 12 to 15 m in the central part, progressively decreasing towards the borders of the deposit (Fig. 5). Six representative stratigraphic cross sections selected along a N-S traverse (location marked by arrows I to VI in Fig. 6), from the center to the border of the lacustrine system, have been drawn in Fig. 7. Sepiolite occurs together with different types of sedimentary rocks within the Intermediate Unit. Clay layers with diverse colors dominate in this unit, intercalated with carbonates (marly mudstones, marls, dolostones, and limestones) which are more abundant towards the top and the margins. Several layers of chert associated with sandy mudstones and arkosic sands of fluvial origin occur in the margins of the deposit.



Figure 5. Vicálvaro sepiolite quarry (April 27th, 2010)

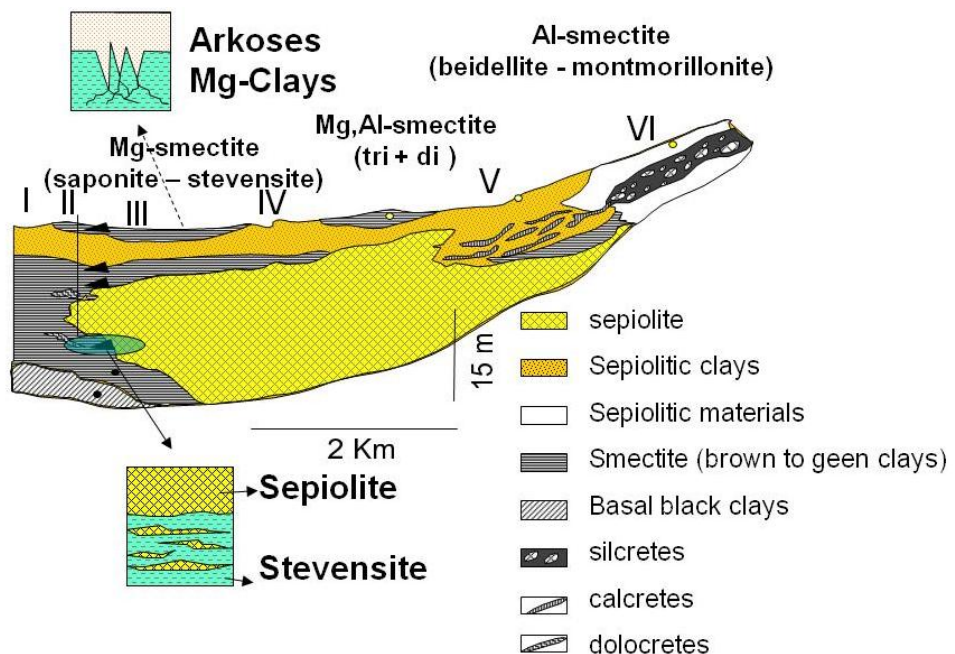


Figure 6: Typical distribution of clayey materials along a lacustrine episode of the Vicálvaro deposit. After Cuevas et al. (1995), Leguey et al. (1995), Ramirez et al. (1996), Cuevas et al. (2003).

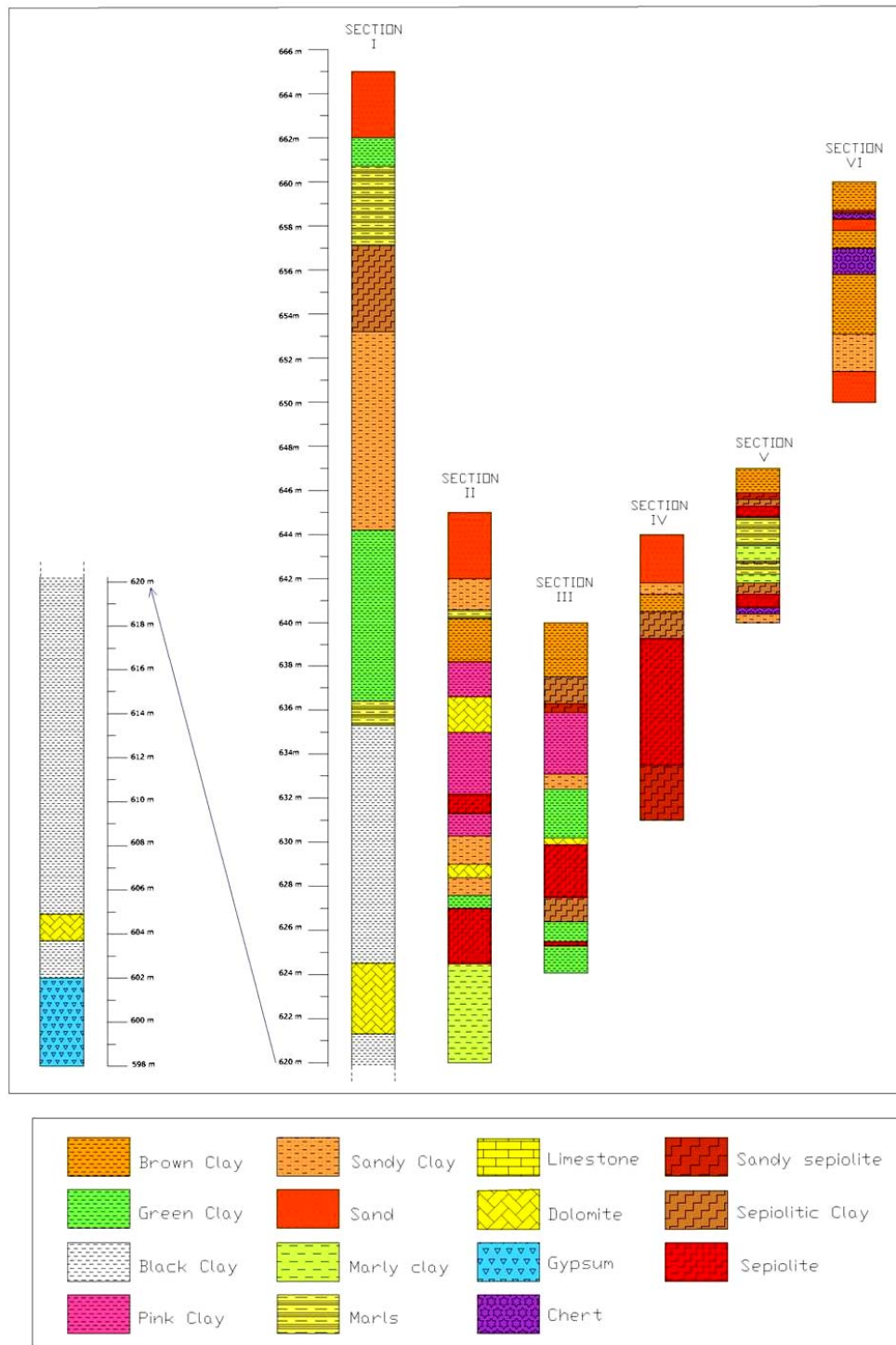


Figure 7. Six representative stratigraphic cross sections selected along a N-S traverse (location shown in Figures 5 and 6).

The base of section I contains massive fibrous gypsum layers interbedded with centimeter-scale layers of black mudstones. These mudstones, rich in organic matter, become the dominant lithology towards the middle part of the sequence, where they occur intercalated with grayish to white layers of marls (up to 1.5 m thick), which in turn contain abundant carbonate veinlets and small nodules. These materials are overlain by marly mudstones of different colours (gray, bluish, violet, pink and green) with intercalations of white limestone, capped by a thick layer of arkosic sands. The top of this layer of sands contains laminated marls with whitish sepiolite clay.

The mineral assemblage in the black mudstones is formed by illite, kaolinite, and smectite, along with quartz, feldspar and gypsum. In samples containing a high proportion of gypsum, feldspar is lacking, and only traces of smectite are detected. Both phases are progressively more abundant as gypsum contents decrease. Gray and whitish layers are practically devoid of kaolinite and show an important decrease of illite. Conversely, these layers show a progressive increase in smectite contents (up to 50 wt%) along with dolomite enrichment within the interbedded marly layers (40 wt% dolomite) and carbonate lenses (up to 100 wt%). Magnesite (12-17 wt%) has been recognized in layers with illite contents higher than those of smectite. The layers of coloured mudstones show smectite contents up to 90 wt%. The clay fraction of the laminated dolomitic marls from the top of the section is formed by smectite (30-58 wt%) and sepiolite (20-35 wt%).

The sepiolite-rich layers are very difficult to correlate with each other because of their irregular vertical and lateral development. At the base of sections II, III and IV, pure sepiolite layers with thicknesses of 1.3, 4 and 7 m, respectively, overlie dolomitic marly mudstones. This remarkable increase in the thickness of the sepiolite layers towards the north is associated with a decrease in the smectite content (which constitute 60-90 wt% of the green mudstones), and with the absence of dolomite. Calcite (1-15 wt%) occurs towards the top of these sections together with smectite in the pink mudstones and with sepiolite in

the sepiolite clays (sepiolite 60-80 wt%). Small proportions of palygorskite and zeolites (heulandite-clinoptilolite; Cuevas et al., 1995) are also recognized in the pink mudstones of section III and in the brown mudstones of section II, respectively.

Towards the border of the deposit (section V), several thin layers (0.2-0.5 m thick) composed of sepiolite (sepiolite > 80 wt%) and sepiolite clay alternate with marls and marly mudstones. The sepiolite layer at the base lies on a chert bed, which in turn contains chalcedony nodules coated by laminar sepiolite ("mountain leather").

Finally, sands and sandy mudstones with intercalated chert masses occur in topographically higher levels in section VI. These layers commonly contain less than 30 wt% sepiolite (sepiolite materials), although in some ferruginous sands (containing hematite and siderite) it may reach up to 60 wt%. The chert is composed of opal-CT with minor quartz, feldspar, and traces of illite and smectite.

The clay mineralogy evolution from section I to VI represents the transition from a permanent lacustrine environment, in which authigenic smectite (saponite-stevensite) predominates, to an ephemeral shallow lake environment. Sepiolite is formed in such transitional environments, alternating with carbonates and clayey sediments with dioctahedral smectites.

Gypsum, silica minerals and/or Mg-clays are found together with sepiolite in the sediments studied in the Barajas area. However, these sediments are marked by the absence of calcite. Several layers of sepiolite can be recognized in the studied location. These layers are related to those of the Vicálvaro sepiolite deposit to the north (Fig. 3). The materials are primarily brown to gray-green clays, with pale-beige layers of sepiolitic composition, and nodular to network carbonate sediments (marls and clayey marls). Lithological and

mineralogical features of a sequence studied in the Barajas area are shown in Fig. 8 in which three sepiolite layers, 2 to 2.5-m thick, are identified.

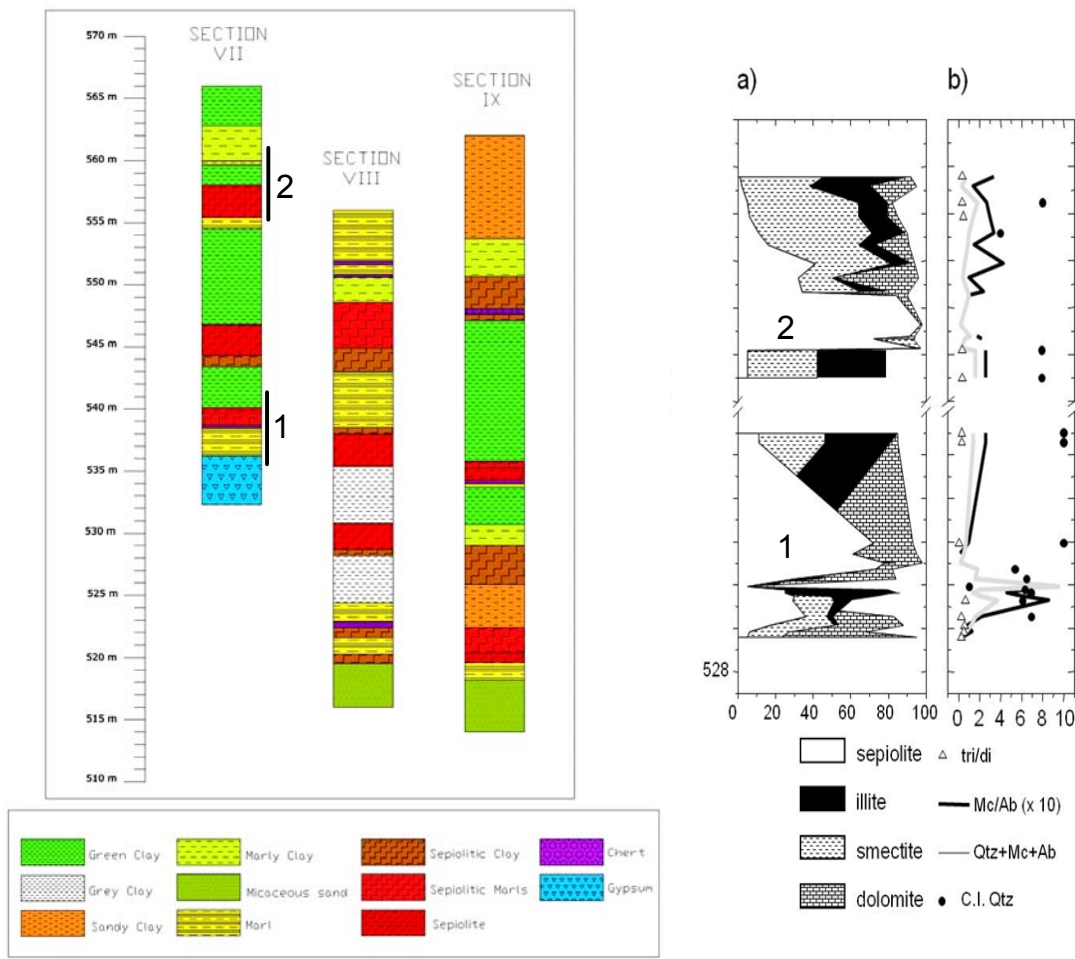


Figure 8: Lithology of the studied sedimentary sequence at Barajas (after Leguey et al., 2010). Mineralogy and related parameters determined in section VII at the Barajas area. a) Plot of bulk mineralogy evolution in the upper and lower levels. b) Evolution of quartz, feldspars and tri-octahedral/dioctahedral ratio (tri/di) in clay minerals, excluding sepiolite. Legend: Mc/Ab: microcline/albite ratio; Qtz+Mc+Ab: sum of quartz and feldspars. C.I. Qtz: quartz crystallinity index.

The evolution in bulk mineralogy along the two studied sepiolite levels is characterized by a sharp increase of sepiolite concentration in the materials overlying the detrital sediments (Fig. 8). However, in the lower level a thin (10 cm) chert bed is located below sepiolite. The detrital beds are mainly composed of illite, smectite, kaolinite (only in the upper level), quartz and feldspars. Dolomite content decreases in these beds, and it sharply rises as sepiolite contents start to decrease upwards. Both, sepiolite and dolomite were detected in minor quantities in the lutites that capped the lower and upper levels.

Changes in clay minerals chemistry can be followed in the sedimentary sequences. The clay minerals at the base of the upper level are composed of illite and smectite, both tri- and dioctahedral. However, the clay minerals at the top show higher smectite contents with similar tri-di ratio than the clays at the base, but with the presence of Fe-illite (1.51 \AA) when the sepiolite content decreases. The lowest amounts of tri-octahedral smectite and microcline are found in samples where sepiolite contents are significantly increased. The gap in microcline/albite ratio between 549 and 550 m coincides with a minimum in microcline and trioctahedral smectite and at the same time with a maximum in sepiolite concentration. The lowest amounts of tri-octahedral smectite, biotite, illite and microcline are found in samples where sepiolite contents are significantly increased. This depletion in K-minerals within the sepiolite rich sediments has been interpreted by Leguey et al. (2010), as a signature for biological activity.

2.2. SOUTHERN AREA

Mg-rich clays in this area of the Madrid basin are associated with two lithostratigraphic units included within the above mentioned Miocene Intermediate Unit, namely the *Green Clays Unit* and the *Fine-grained Sandstones with Sepiolite, Chert and Carbonate Unit* (Fig. 9 and 10) (García-Romero, 1988; García-Romero et al. 1990). Their main characteristics are outlined below.

Green Clays Unit

This unit is restricted to two outcrops (inselbergs) within this southern area, close to the villages of Cabañas de la Sagra and Villaluenga (Figure 10 and 11). Sedimentologically, it corresponds to mud flat facies deposited along the margins of the evaporite core of the basin. Details of stratigraphic sections are shown in Fig. 12 (Cuevas et al., 1993). This unit was deposited in a low-energy sedimentary environment, as revealed by the absence of coarse-grained sediments. Its thickness is up to 60 m and it lies over the so-called *La Sagra Red Clays Unit*, which can be correlated with the Miocene Lower Unit (Fig. 9 and 10). The La Sagra Red Clays Unit (composed of up to 90% sheet silicates; mainly illite, dioctahedral smectite, and minor kaolinite and/or chlorite) is economically important in the area, since it provides the raw material for numerous brick-making industries.

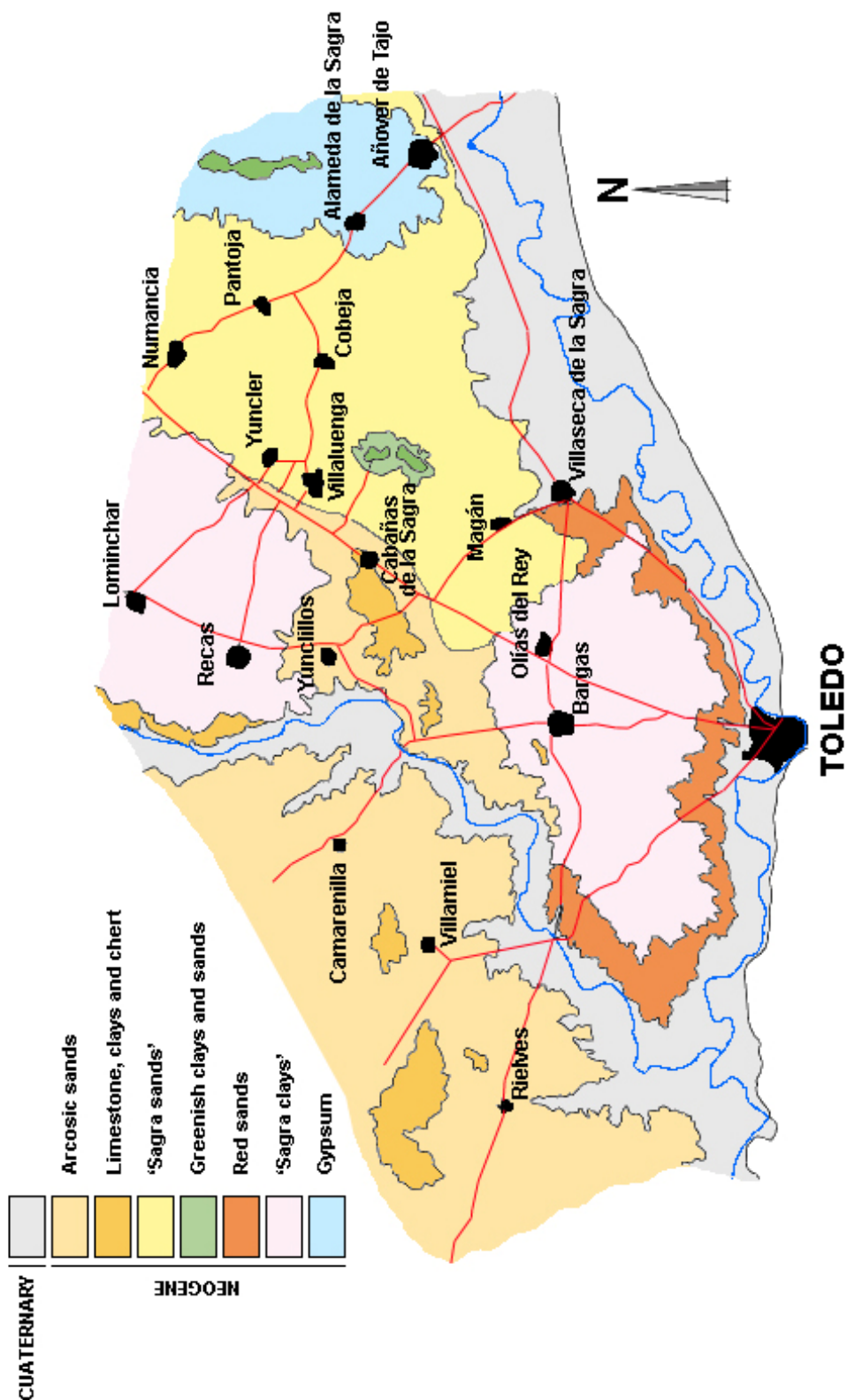


Figure 9. Geological map of the "La Sagra" area (modified after Garcia-Romero et al., 1990)

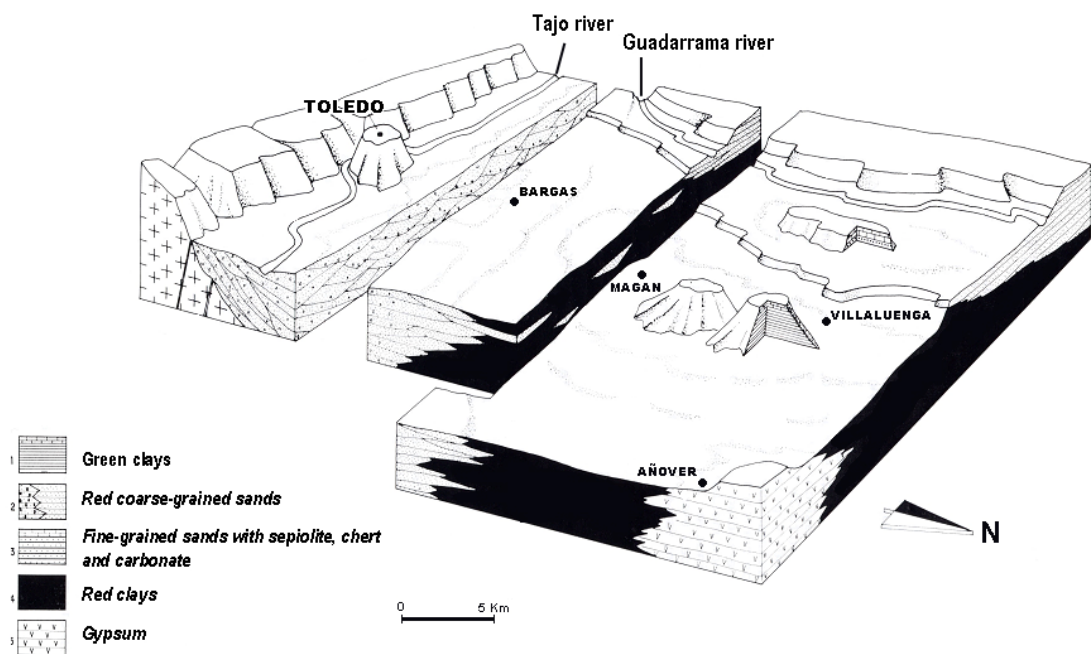


Figure 10. 3-D section of the southern area of the Madrid basin.
After García-Romero et al. (1990)



Figure 11. Outcrops of the Green Clays Unit

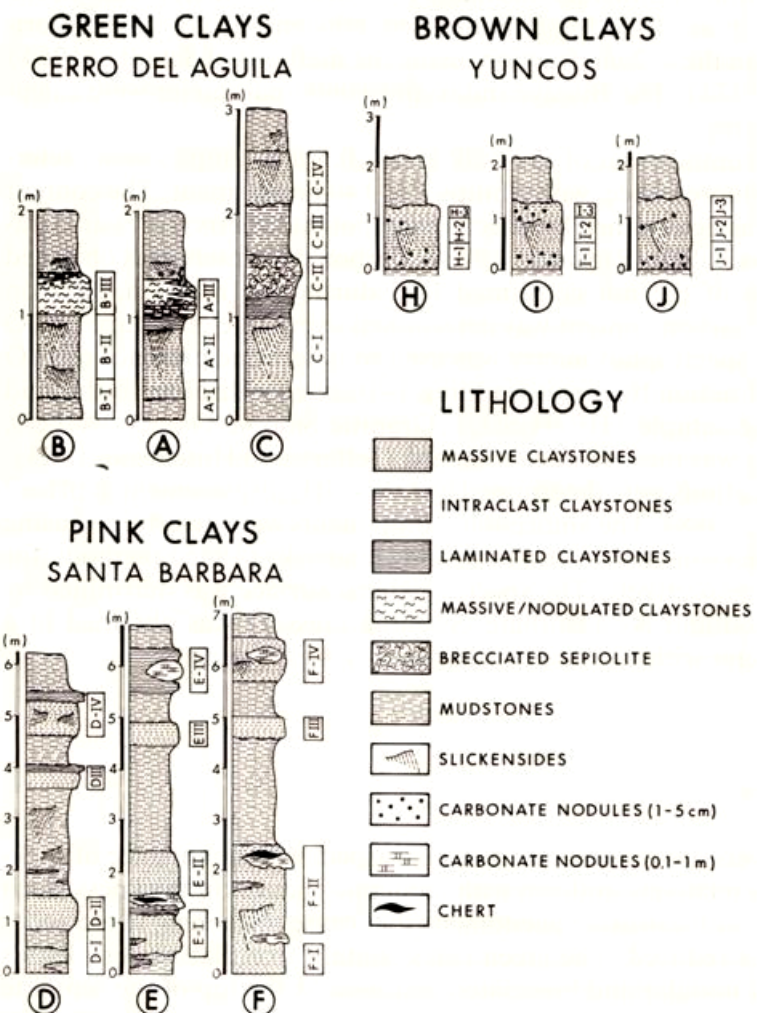


Figure 12. Stratigraphic sections from bentonite quarries in the SE of Madrid Basin. After Cuevas et al. (1993)

The *Green Clays Unit* contains the important bentonite deposits of the Madrid Basin (Fig. 13). This unit consists of massive green bentonite clays, in which trioctahedral smectite (principally saponite) makes up to 100 wt% of the clay fraction (Brell et al., 1985, García Romero, 1988). Minor illite (up to 10 wt%) and kaolinite may appear. At the top of this unit, dolomitic marls or dolostones, locally silicified, may appear. Some beds of micaceous sands showing crossed or parallel lamination, also occur towards its lower middle part. Biotite and chlorite are the only phyllosilicates in these sands. A very significant feature of this unit is the presence of some pinkish clay levels which appear as massive clays, irregular pinkish lenses with sepiolite, of nodular and brecciated

textures. The detailed description of these pink nodules and layers is given below.



Figure 13. Bentonite quarry (Cerro del Águila)

The pink clay levels (Fig. 14), interbedded within the Green Clays Unit, have a massive aspect and pink colour. Sometimes they contain green mudstone intercalations and isolate carbonate nodules. Towards the top the levels are darker and laminated. They retain bioturbation features with irregular concrections and slickensides stained by iron oxides.



Figure 14. Pink clay levels (marked by arrows) interbedded within green clays.

Fine-grained sands with sepiolite, chert and carbonate Unit

This unit comprises an alternation of brownish clays and silty sands levels with total thickness ranging from about 4 to 20 m. The sedimentary environment of this unit corresponds to the distal parts of alluvial fans, in which sedimentation occurred below a seasonal shallow water column. Clayey levels are widespread close to the center of the basin, whereas the silty sands levels are dominant to the margins of the basin. Clayey levels consist of different proportions of sepiolite and trioctahedral smectite, being occasionally composed by pure sepiolite or smectite levels. Sepiolite beds may reach up to 1-3 m (Fig. 15). They constitute the important deposits of the southern part of the Madrid Basin. The top of the unit is outlined by the occurrence of levels in which sepiolite is associated with carbonate (dolomite) and chert (Figs. 16 and 17). It also contains quartz (5-40 wt%), and plagioclase (5-35 wt%), and illite and kaolinite (García-Romero, 1988). Locally, the unit may contain zeolites (mordenite and heulandite) (Brell et al. 1985; Bellanca et al. 1992; Bustillo and García-Romero, 2003).

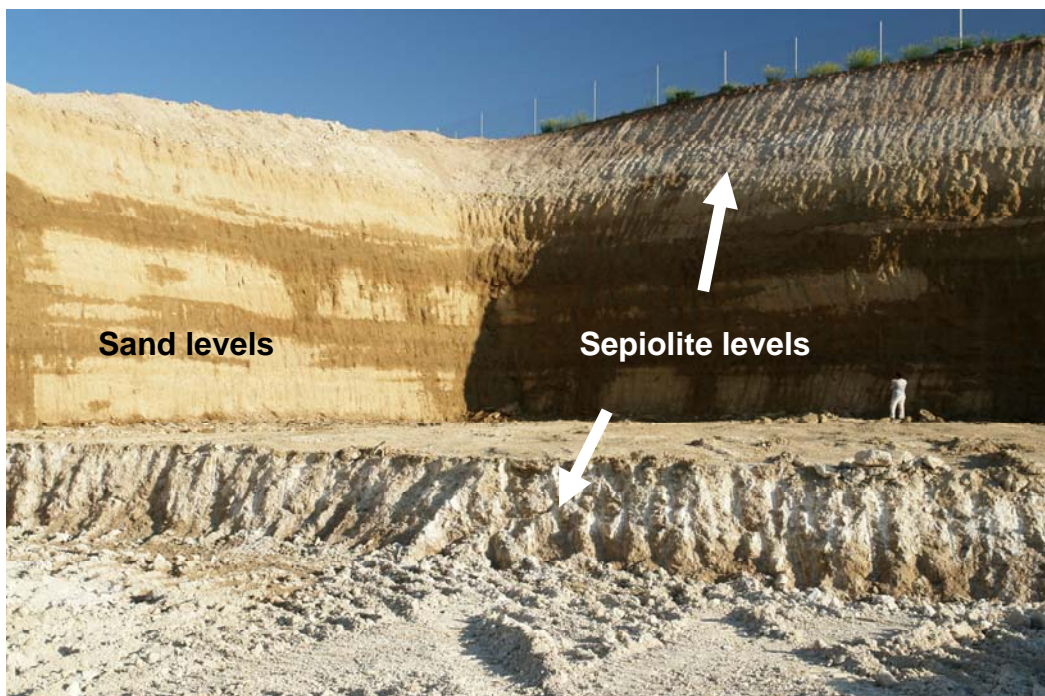


Figure 15. Sepiolite quarry (Cabañas de la Sagra)



Figure 16. Detail of the sepiolite levels (Cabañas de la Sagra)



Figure 17. Details of the chert levels

3. MINERALOGY OF MAGNESIUM CLAYS

Bentonite deposits

The bentonite deposits are composed of phyllosilicates (75-90%) with minor feldspar and quartz. Most of these phyllosilicates are trioctahedral smectites and <10% illite. Small amounts of kaolinite are sometimes present.

Scanning electron microscopy (SEM) images show that the smectite fabric is completely isotropic, being formed by a random array of particles that display a flocculated fabric. The smectite particles have a flaky morphology which shows edge-to-face, and edge-to-edge contacts with curly edges (Fig. 18a). Such laminar aggregates are often associated with fibrous edge morphologies (Fig. 18b), probably new formed, originated by curling of laminar particles of smectite at their edges as seen by transmission electron microscopy (TEM) observations. Illite occurs as platy-like particles corresponding to relatively thick and well developed crystals. TEM micrographs revealed the coexistence of smectite, illite and interstratified illite-smectite (IS) (De Santiago et al., 1998).

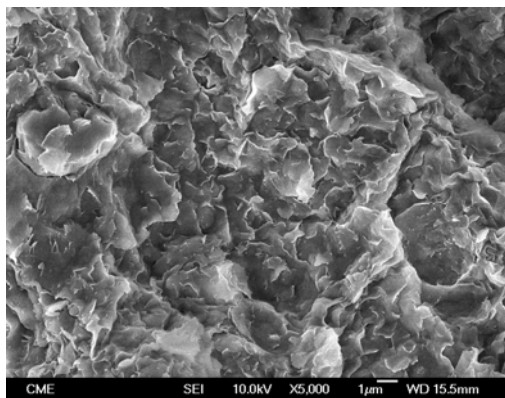


Figure 18a. Morphology of smectite particles

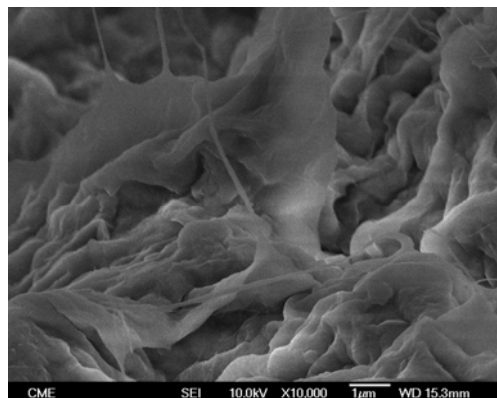


Figure 18b. Smectite particles with associated fibrous morphologies

Analytical electron microscopy (AEM) analyses of bentonite samples show a continuous range of compositions from dioctahedral Al-mica to trioctahedral Mg-smectite, mainly saponite. Table 1 shows the mean structural formulae for smectite from this Unit.

De Santiago et al. (1998) stated that bentonites from the Green Clays Unit were essentially new formed. In addition to these new formed smectites, small amounts of detrital dioctahedral illite became unstable in such Mg-rich environments and underwent a weathering process that eventually resulted in the formation of smectite. Cuevas et al. (2003) discussed the nature of the saponitic clays associated with sepiolite in the Vicálvaro deposit. X-ray diffraction (XRD) and infra-red (IR) data demonstrated that all of the Mg-smectite materials are mostly composed of a complex mixture of stevensite, saponite and mica-type minerals. Although the presence or absence of saponite could not be strictly elucidated, stevensite was a significant component of these magnesium smectites. These results are in close agreement with the mechanism of topotactic overgrowth of stevensite on pre-existent phyllosilicate templates in saline-alkaline lake systems as suggested by Banfield et al. (1991).

Pink Clays

XRD patterns of pink clays (Fig. 19) show a very broad diffraction effect at low angles. This XRD pattern is composed of (hk0) and (00l) broad and asymmetrical bands instead of discrete reflections. This may be related to the lack of three-dimensional periodicity due to arbitrary rotation or sliding between the layers, giving rise to extensive stacking disorder (Martín de Vidales *et al.*, 1991, De Santiago *et al.* 2000). These authors assumed that this phenomenon was related to particle size and textural features. Furthermore, partial hydration of the sample can produce the enlargement of the basal reflections. The *b*-axis dimension, estimated from the (060) reflection is 9.18 Å, which indicates the trioctahedral character. No phases other than clay minerals were detected (De Santiago *et al.*, 2000).

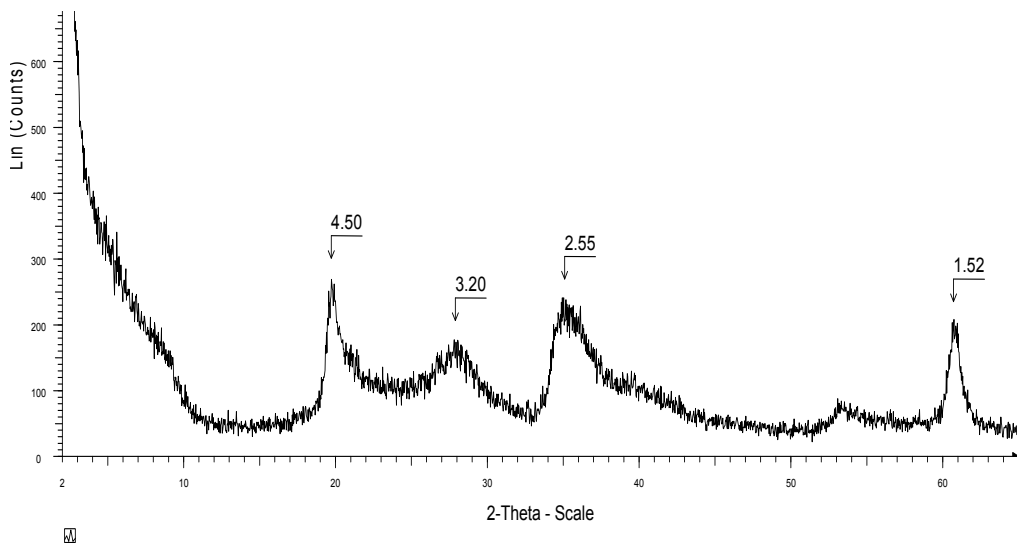


Figure 19. XRD pattern of randomly oriented powder of pink clay.

Figure 20 shows an XRD pattern of the oriented aggregate of the clay fraction < 2 µm (air-dried, solvated with ethylene-glycol, and heated to 550 °C). Low angle scattering is observed in all the cases. This band may be produced by different interlayered phases in the sample. Samples solvated with ethylene-

glycol swell slightly. Also, when heated at 550 °C, the d-spacing values decrease slightly. The 002 and higher order peaks are missing in the pattern indicating the lack of periodic stacking of layers along the [00l] direction. The absence of well defined 00l reflections makes impossible the calculation of the crystallinity index or average crystal size. Although the smectitic nature of the clays and the trioctahedral character of the mineral can be determined by XRD, the broad reflections suggest that these materials have barely coherent domains with a very small number of layers per particle.

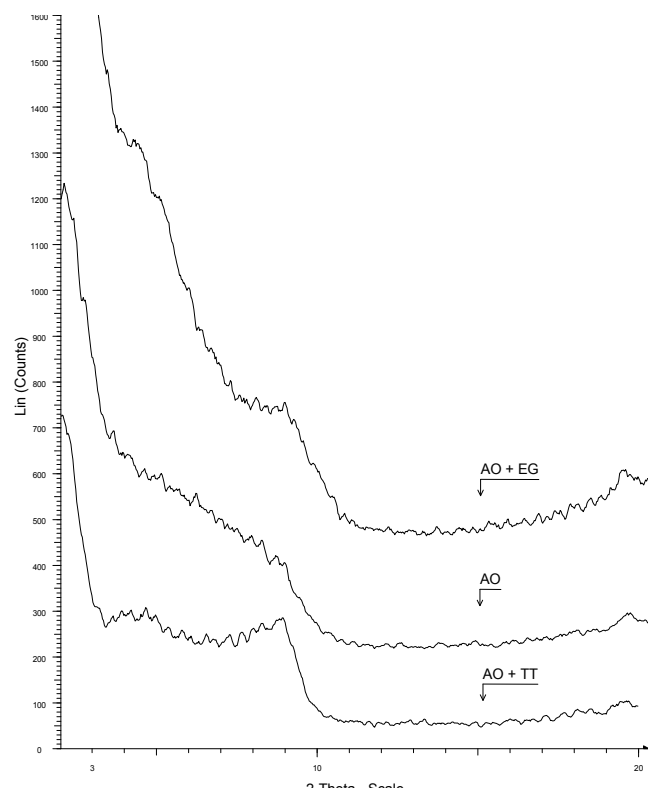


Figure 19. X-ray diffraction pattern of the oriented aggregate (< 2 µm) of a sample of pink clays (AO: air-dried, AO+EG: solvated with ethylene-glycol, and AO+TT: heated to 550 °C).

A nearly isotropic fabric is observed by SEM. Samples are formed by random (non-oriented) arrays of very small smectite particles showing open structures with pseudo-polygonal voids “cornflake” and “honey-comb” microstructure (Fig. 21). Such a microstructure is formed by smectite particles with curled edges, which keep edge-to-face, and edge-to-edge contacts. Elsewhere, these clay particles are usually inter-connected forming flocks or aggregate structures with spherical morphologies (cellular texture) separated by voids of varying sizes and shapes.

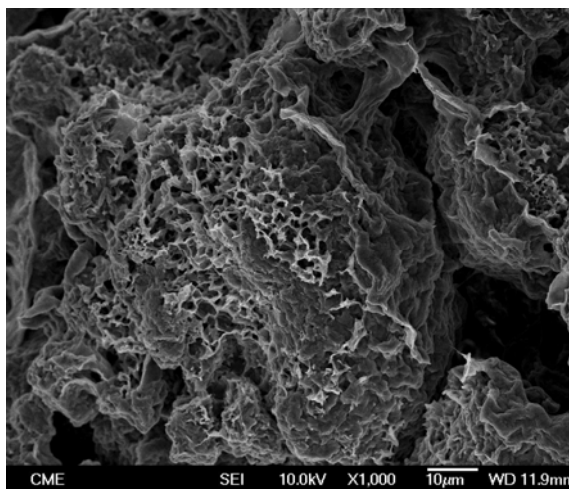


Figure 21a. Pink clay particles morphology

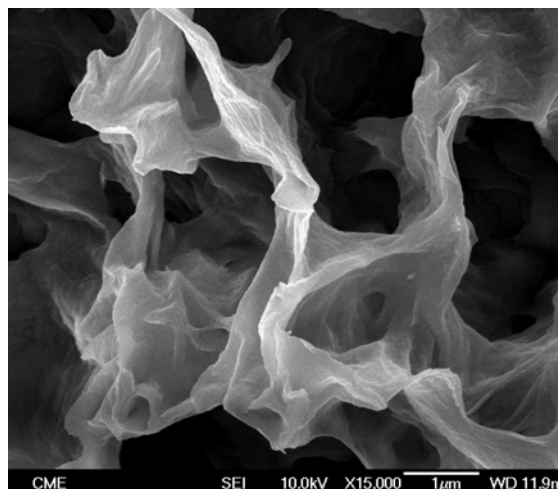


Figure 21b. Detail of the morphology of smectite from pink clay

TEM photomicrographs show broad, poorly-defined fringes varying from 10 to 18 Å thick. The particles have wavy, anastomosing, and discontinuous lattice-fringe images (Fig. 22) with a high number of edge dislocations and changes in image contrast along the layers, owing to small orientation changes in the crystal. The heterogeneity and wavy structure of the lattice fringes are consistent with sample formation in relatively shallow water environments where crystallization occurred relatively rapidly at low temperatures.

In addition, TEM photomicrographs show a common structure of hollow-packed spheres (Fig. 22), with apparent diameters ranging from 50 to 1000 Å. Some sphere walls display a concentric layered structure. This cellular texture

resembles descriptions of primitive clay precursors forming from glasses, gels, or weathering of previous minerals (De Santiago et al. 2000).

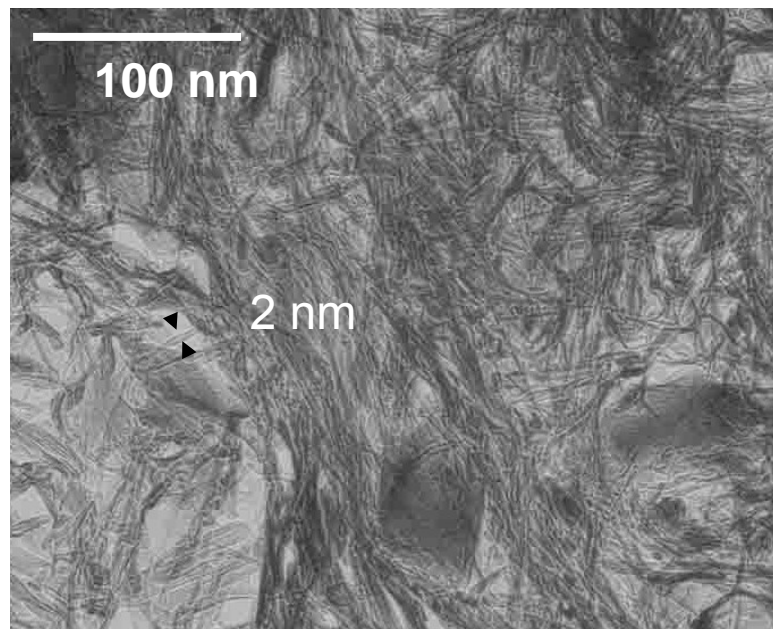


Figure 22. Morphology of pink clay particles.

The average structural formulae calculated from the AEM analyses of pink clays are listed in table I. Several authors had described this mineral as a mixed-layer Kerolite-stevensite (Martín de Vidales et al., 1991; Cuevas, 1992; Pozo and Casas, 1992, 1995; Pozo et al., 1999; Pozo and Casas, 1999). Afterwards, De Santiago et al. (2000) stated that they can be ascribed to stevensite with an extremely low cation exchange capacity (generated by a deficiency of octahedral cations in the structure, and not by isomorphic substitutions).

Sepiolite deposits

Sepiolite from the Madrid basin has been mostly quarried at the Vicálvaro deposit. It is not unusual to find layers with whitish creamy colors composed of sepiolite (>90 wt % grade). This is common also in Cabañas deposit and in the known reserves actually buried under the T4 terminal of the Madrid-Barajas Airport. The X-ray diffraction patterns of bulk materials either from Vicálvaro-Barajas and Cabañas de la Sagra, without any pretreatment, show profiles characteristic of single mineral sepiolite reflections (see patterns in the Field trip stop section). Some of them can be refined by the Rietveld method (Ruiz, 2010, unpublished; Fig. 23), using an ideal sepiolite chemistry. In fact, this ideal composition can be confirmed by bulk chemical analysis from which the structural formula calculation yielded an ideal Si/Mg atomic ratio of 12/8 and a significant F content in OH positions (Table 1).

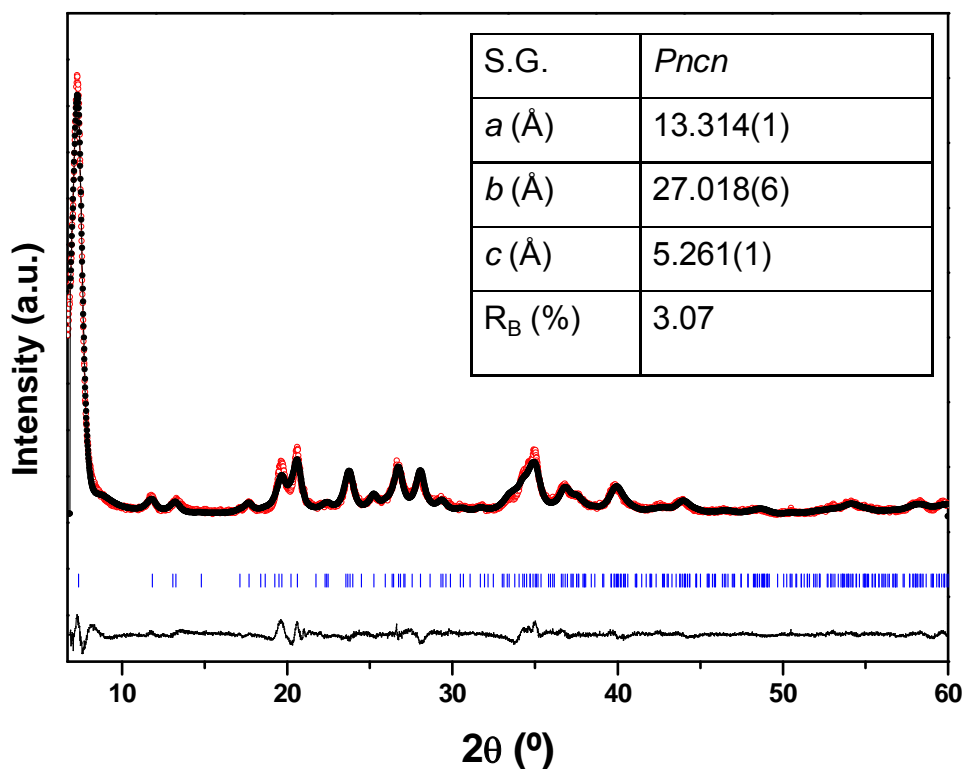


Figure 23. Rietveld refinement of the Vicálvaro Sepiolite and cell parameters.

SEM images (Fig. 24) reveal the characteristic fibrous morphology of this mineral. The aggregates grow as dense fibre masses connected to each other in the fibrous clays beds, or enmesh and sprout out from the surface, and filling voids totally or partially. The fibers are long, having an average length of 1-2 μm , and their diameters may vary between 0.15-0.5 μm (Figure 24 a and b).

Sepiolite at the Barajas area lies mixed or intercalated within dolomitic marls in which calcite is absent. Figures 24 c, d, e, and f show dolomitic biomorphs in which sepiolite intergrowths are evidenced. This has aimed research studies focused to look for the relation of sepiolite formation to biomineralization processes (Leguey et al., 2010). The potential role of biomineralization in the formation of these high-grade sepiolite deposits depends on two factors: (1) specific organic-inorganic interactions and (2) the highly porous nature of the sepiolite precursor dolomite (Figure 24 e) during the diagenetic evolution of these sediments. These diagenetic processes consisted in the dissolution of dolomite relics and the formation of new sepiolite in a highly porous and compact network.

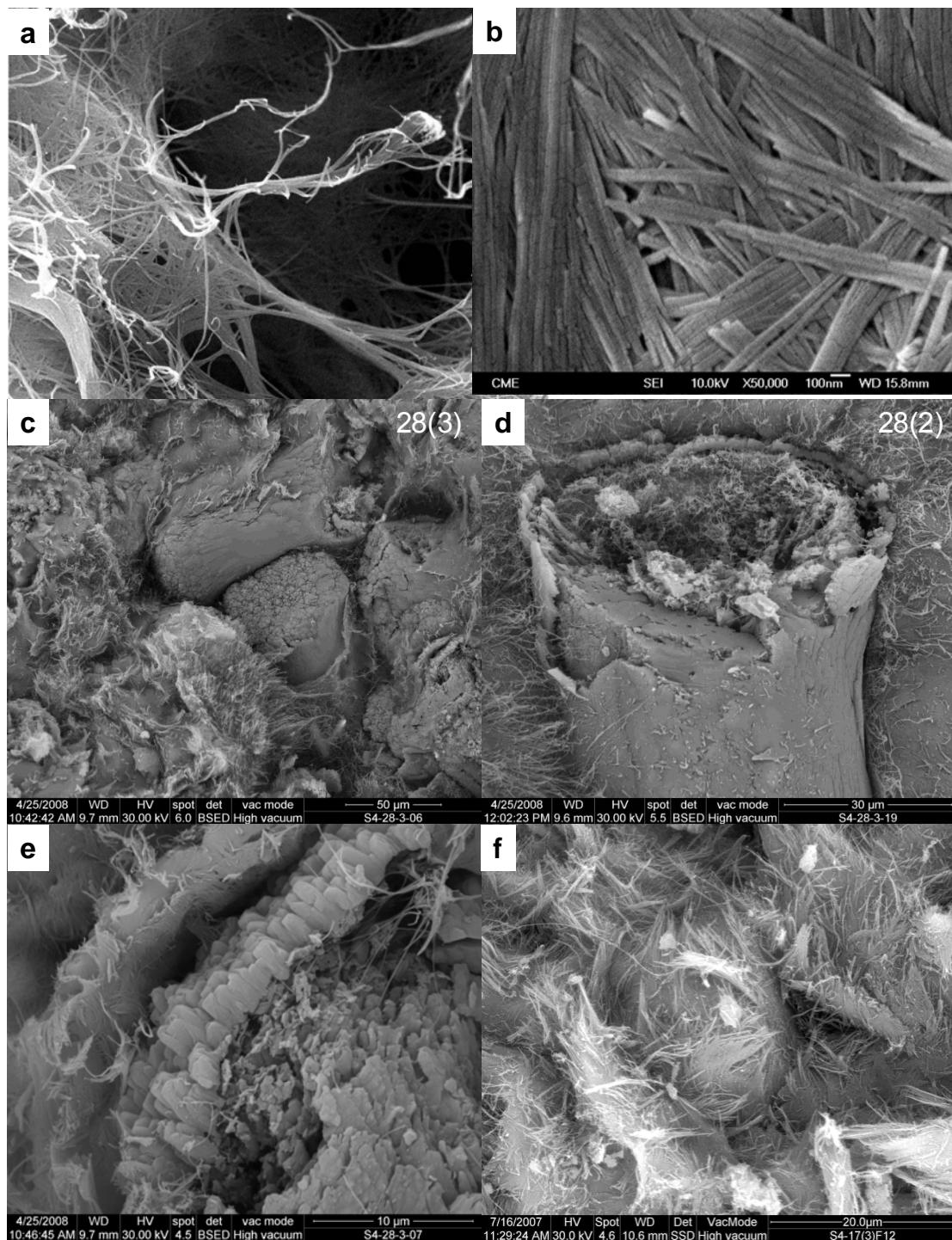


Figure 24. a: SEM micrograph of sepiolite from Vicálvaro. b: SEM micrograph of sepiolite from Cabañas de la Sagra. c: cylindrical biomorphs of dolomite in the sepiolite matrix; d: mixed sepiolite-dolomite cylinder with external dolomite crust; e: oriented crystals of dolomite (crust) normal to the cylinder axis and internal lamellar structure; f: Sepiolite ovoid-like texture.

Table 1 : Crystal Chemistry of Mg-Clays from the Madrid basin

Unit	Locality	R	Mineralogy	Structural formula
Green Clays	Cerro del Águila / Magán	1	Saponite	$\text{Si}_{7.4}\text{Al}_{0.6}(\text{Al}_{0.4}\text{Mg}_{5.4}\text{Fe}^{3+}_{0.05}\text{Fe}^{2+}_{0.15})\text{X}^+_{0.3}\text{O}_{20}(\text{OH})_4$
		2	Saponite	$\text{Si}_{7.52}\text{Al}_{2.80}(\text{Al}_{0.88}\text{Mg}_{3.62}\text{Fe}^{3+}_{0.52})\text{Ca}_{0.1}\text{K}_{1.38}\text{O}_{20}(\text{OH})_4$
		3	Saponite	$\text{Si}_{7.33}\text{Al}_{0.67}(\text{Al}_{0.33}\text{Mg}_{5.00}\text{Fe}^{3+}_{0.25}\text{Ti}_{0.02})\text{Ca}_{0.40}\text{K}_{0.05}\text{O}_{20}(\text{OH})_4$
			Saponite	$\text{Si}_{7.26}\text{Al}_{0.74}(\text{Al}_{0.52}\text{Mg}_{4.55}\text{Fe}^{3+}_{0.35}\text{Ti}_{0.03})\text{Ca}_{0.39}\text{K}_{0.13}\text{O}_{20}(\text{OH})_4$
		2	Illite	$\text{Si}_{6.18}\text{Al}_{0.18}(\text{Al}_{3.58}\text{Mg}_{0.46}\text{Fe}^{3+}_{0.16})\text{K}_{1.58}\text{O}_{20}(\text{OH})_4$
			Mixed-layer	$\text{Si}_{6.70}\text{Al}_{1.30}(\text{Al}_{1.1}\text{Mg}_{3.9}\text{Fe}^{3+}_{0.46})\text{Ca}_{0.06}\text{K}_{0.5}\text{O}_{20}(\text{OH})_4$
Pink Clays	Cerro Aguila	4	Stevensite	$\text{Si}_{8.01}(\text{Al}_{0.36}\text{Mg}_{4.76}\text{Fe}^{3+}_{0.11}\text{Fe}^{2+}_{0.03})\text{Mg}_{0.45}\text{Na}_{0.01}\text{K}_{0.01}\text{O}_{20}(\text{OH})_4$
	Santa Bárbara	3	Stevensite	$\text{Si}_{7.69}\text{Al}_{0.31}(\text{Mg}_{5.61}\text{Al}_{0.09}\text{Fe}^{3+}_{0.08})\text{Ca}_{0.29}\text{K}_{0.01}\text{O}_{20}(\text{OH})_4$
	Esquivias	5	Kerolite/Stevensite	$\text{Si}_{7.88}\text{Al}_{0.12}(\text{Al}_{0.02}\text{Fe}^{3+}_{0.03}\text{Ti}_{0.01}\text{Mg}_{5.88})\text{Na}_{0.02}\text{Li}_{0.02}\text{Sr}_{0.06}\text{O}_{20}(\text{OH})_4$
	Esquivias	6	Kerolite	$\text{Si}_8(\text{Al}_{0.1}\text{Fe}^{3+}_{0.05}\text{Mg}_{5.66})\text{Na}_{0.04}\text{Ca}_{0.04}\text{Sr}_{0.05}\text{O}_{20}(\text{OH})_4$
				$\text{Si}_{7.90}\text{Al}_{0.1}(\text{Al}_{0.03}\text{Fe}^{3+}_{0.03}\text{Ti}_{0.01}\text{Mg}_{5.89})\text{Na}_{0.01}\text{Ca}_{0.02}\text{Sr}_{0.03}\text{O}_{20}(\text{OH})_4$
	Vicálvaro	7	Stevensite	$\text{Si}_{7.94}\text{Al}_{0.06}(\text{Mg}_{5.34}\text{Li}_{0.08}\text{Al}_{0.15}\text{Fe}^{3+}_{0.09}\text{Ti}_{0.01})\text{Ca}_{0.18}\text{Na}_{0.08}\text{K}_{0.01}\text{O}_{20}(\text{OH})_4\text{F}_{0.53}$
	Vicálvaro		Saponite-stevensite	$\text{Si}_{7.51}\text{Al}_{0.49}(\text{Mg}_{4.95}\text{Al}_{0.43}\text{Fe}^{3+}_{0.16}\text{Ti}_{0.01})\text{Ca}_{0.35}\text{K}_{0.08}\text{O}_{20}(\text{OH})_4$
	Pinto	5	Kerolite/Stevensite	$\text{Si}_{7.80}\text{Al}_{0.20}(\text{Al}_{0.06}\text{Fe}^{3+}_{0.06}\text{Ti}_{0.01}\text{Mg}_{5.56})\text{Na}_{0.06}\text{K}_{0.02}\text{Li}_{0.02}\text{Sr}_{0.20}\text{O}_{20}(\text{OH})_4$
Sepiolite	Barajas	8	Sepiolite	$\text{Si}_{12.041}(\text{Al}_{0.05}\text{Mg}_{7.845})\text{O}_{30}(\text{OH})_{3.352}\text{F}_{0.648}(\text{OH}_2)_4$
	Vicálvaro	9	Sepiolite	$\text{Si}_{12.023}(\text{Mg}_{7.955})\text{O}_{30}(\text{OH})_{3.139}\text{F}_{0.8604}(\text{OH}_2)_4$
	Batallones	10	Sepiolite	$\text{Si}_{11.81}\text{Al}_{0.19}(\text{Al}_{0.68}\text{Fe}^{3+}_{0.28}\text{Mg}_{6.1}\text{Ti}_{0.13})\text{Ca}_{0.18}\text{K}_{0.12}\text{Na}_{0.04}\text{O}_{30}(\text{OH})_4(\text{OH}_2)_4$
	Vicalvaro		Sepiolite	$\text{Si}_{11.77}\text{Al}_{0.23}(\text{Al}_{0.27}\text{Fe}^{3+}_{0.23}\text{Mg}_{7.22}\text{Ti}_{0.13})\text{Ca}_{0.10}\text{K}_{0.06}\text{Na}_{0.01}\text{O}_{30}(\text{OH})_4(\text{OH}_2)_4$
	Vallecas		Sepiolite	$\text{Si}_{11.84}\text{Al}_{0.16}(\text{Al}_{0.25}\text{Fe}^{3+}_{0.06}\text{Mg}_{7.35}\text{Ti}_{0.03})\text{Ca}_{0.05}\text{K}_{0.08}\text{Na}_{0.06}\text{O}_{30}(\text{OH})_4(\text{OH}_2)_4$
	Yuncos		Sepiolite	$\text{Si}_{12}(\text{Al}_{0.27}\text{Fe}^{3+}_{0.03}\text{Mg}_{7.45})\text{Ca}_{0.02}\text{K}_{0.01}\text{Na}_{0.03}\text{O}_{30}(\text{OH})_4(\text{OH}_2)_4$
	Esquivias	5	Sepiolite	$\text{Si}_{11.95}\text{Al}_{0.05}(\text{Al}_{0.05}\text{Fe}^{3+}_{0.02}\text{Mg}_{7.88})\text{Ca}_{0.02}\text{K}_{0.02}\text{Na}_{0.02}\text{O}_{30}(\text{OH})_4(\text{OH}_2)_4$
Palygorskite	Esquivias	10	Palygorskite	$\text{Si}_{7.95}\text{Al}_{0.05}(\text{Al}_{0.92}\text{Fe}^{3+}_{0.14}\text{Mg}_{3.34})\text{Ca}_{0.03}\text{K}_{0.04}\text{O}_{20}(\text{OH})_2(\text{OH}_2)_4$
			Palygorskite	$\text{Si}_{7.92}\text{Al}_{0.08}(\text{Al}_{1.14}\text{Fe}^{3+}_{0.18}\text{Mg}_{2.92})\text{Ca}_{0.04}\text{K}_{0.04}\text{Na}_{0.06}\text{O}_{20}(\text{OH})_2(\text{OH}_2)_4$

R : References. 1. Galán et al. (1986); 2. De Santiago et al., (1998); 3. Cuevas et al., (1993); 4. De Santiago et al., (2000); 5. Pozo et al., (1999); 6. Pozo and Casas (1999); 7. Cuevas et al. (2003); 8. Leguey et al., (2010); 9. Ruiz (2010); 10. García-Romero and Suárez, (2010).

4. REFERENCES

- ALBERDI, M.T., HOYOS, M., JUNCO, F., LÓPEZ MARTINEZ, N., MORALES, J., SESE, C. Y SORIA, D. 1983. Bioestratigraphie et évolution sedimentaire de l'aire de Madrid. Colloquium Mediterranean Neogene Continental Paleoenvironments and Paleoclimatic evolution. Montpellier, Avril, 12-83.
- ALONSO-ZARZA, A.M., CALVO, J.P. Y GARCÍA DEL CURA, M.A. 1993. Palaeogeomorphological controls on the distribution and sedimentary styles of alluvial systems, Neogene of the NE Madrid Basin (central Spain). In: Alluvial Sedimentation (M. Marzo y C. Puigdefábregas, Eds.), Special Publications International Association Sedimentologists. 17, 277-292.
- ALONSO-ZARZA, A.M., CALVO J.P., SILVA, P.G., TORRES, T. 2004. Cuenca del Tajo. In: Vera, J.A. (Editor), Geología de España. SGE-IGME, 556-561.
- BANFIELD, J.F., JONES, B.F. and VEBLEN, D.R. 1991. An AEM-TEM study of weathering and diagenesis, Albert lake, Oregon: II. Diagenetic modification of the sedimentary assemblage. *Geochimica et Cosmochimica Acta*. 55, 2795-2810.
- BELLANCA, A., CALVO, J.P., CENSI, P., NERI, R. Y POZO, M. 1992. Recognition of lake-level changes in Miocene lacustrine units, Madrid Basin, Spain. Evidence from facies analysis, isotope geochemistry and clay mineralogy. *Sedimentary Geology*. 76, 135-153.
- BRELL, J. M.; DOVAL, M. and CARAMES, M. (1985). Clay minerals distribution in the evaporitic Miocene sediments of the Tajo Basin, Spain. *Mineralogica and Petrographica Acta*. 29, 267-276.

BUSTILLO, M. A., AND ALONSO-ZARZA, A. M. 2007. Overlapping of pedogenesis and meteoric diagenesis in distal alluvial and shallow lacustrine deposits in the Madrid Miocene Basin, Spain. *Sedimentary Geology*. 198, 255–271.

BUSTILLO M^a. A. AND GARCIA-ROMERO E. 2003. Arcillas fibrosas anómalas en encostramientos y sedimentos superficiales: características y génesis. *Revista de la Sociedad Española de Cerámica y Vidrio*. 42, 289-297.

CALVO, J.P., ORDOÑEZ, S., HOYOS, M. Y GARCÍA DEL CURA, M.A. 1984. Caracterización Sedimentológica de la Unidad intermedia del Mioceno en la zona sur de Madrid. *Revista de Materiales y Procesos Geológicos*. 2, 145-176.

CALVO, J.P., ALONSO-ZARZA, A.M., GARCÍA DEL CURA, M.A. 1989. Models of marginal lacustrine sedimentation in response to varied source areas in the Madrid Basin (Central Spain). *Paleogeography, Paleoclimatology, Paleoecology*. 70, 199-214.

CALVO, J.P., JONES, B.J., BUSTILLO, M.A., FORT, R., ALONSO-ZARZA, A.M., KENDALL, C. 1995. Sedimentology and geochemistry of carbonates from lacustrine secuences in the Madrid Basin, Central Spain. *Chemical Geology*. 123, 173-191.

CUEVAS, J. 1992. Caracterización de Arcillas Magnésicas como Materiales de Sellado. Ensayos de Alteración Hidrotermal. Phd. Thesis. ENRESA. Publicación técnica. 04/92. 189p.

CUEVAS, J., PELAYO, M., RIVAS, P. and LEGUEY, S. 1993. Characterization of Mg-Clays from the Neogene of the Madrid Basin and their potential as backfilling and sealing material in high level radioactive waste disposal. *Applied Clay Science*. 7, 383-406.

CUEVAS, J., MEDINA, J.A., CASAS, J., MARTÍN-RUBÍ, J.A., TORRES, M.R., ÁLVAREZ, A. AND LEGUEY, S. 1995. Heulandita asociada a esmectitas-Mg en el yacimiento de sepiolita de Vicálvaro (cuenca Neógena de Madrid). Boletín de la Sociedad Española de Mineralogía. 18, 143-155

CUEVAS, J.; VIGIL DE LA VILLA, R.; RAMÍREZ, S. PETIT, S. MEUNIER, A. and LEGUEY, S. 2003. Chemistry of Mg smectites in lacustrine sediments from te Vicálvaro sepiolite deposit, Madrid Neogene basin (Spain). *Clays and Clay Minerals.* 5, 457-472.

DE SANTIAGO, C.; SUÁREZ, M.; GARCIA ROMERO, E. and DOVAL, M. 2000. Mg-rich smectite “precursor” phase in the Tagus Basin, Spain. *Clays and Clay Minerals.* 48, 366-373.

DE SANTIAGO, C., SUÁREZ, M., GARCIA ROMERO, E. DOMÍNGUEZ DÍAZ, M. C. and DOVAL, M. 1998. Electron microscopic study of the illite-smectite transformation in the bentonites from Cerro del Aguila (Toledo, Spain). *Clay Minerals.* 33, 501-510.

GALÁN, E., ÁLVAREZ, A. and ESTEBAN, M.A. 1986. Characterization and technical properties of a Mg-rich bentonite. *Applied Clay Science,* 1, 295-309.

GARCIA DEL CURA, M.A., ORDÓÑEZ, S. and CALVO, J.P. 1986. La Unidad Salina (Mioceno) en el área de Madrid: características petrológicas y mineralógicas. *Boletín de la Sociedad Española de Mineralogía.* 9, 329-338.

GARCIA-ROMERO, E. 1988. Estudio mineralógico y estratigráfico de las arcillas de las facies centrales del Neógeno del borde sur de la Cuenca del Tajo. Tesis Doctoral. Facultad de Ciencias Geológicas. Universidad complutense de Madrid.

GARCÍA-ROMERO, E., BRELL, J.M., DOVAL, M. and NAVARRO, J.V. 1990. Caracterización mineralógica y estratigráfica de las formaciones neógenas del borde sur de la cuenca del Tajo (Comarca de la Sagra). Boletín geológico y Minero. 101-6, 945-956.

GARCÍA-ROMERO, E., BUSTILLO, A. and SUAREZ, M. 2004. Characteristics of a Mg-palygorskite in Miocene rocks, Madrid basin (Spain). *Clays and Clay Minerals*. 52, 484-494.

GARCÍA-ROMERO, E. and SUAREZ, M. 2010. On the chemical composition on sepiolite and palygorskite. *Clays and Clay Minerals*. 58, 1-20.

GIBBONS, W. and MORENO, T. 2002. The Geology of Spain. The Geological Society. London. 649

JUNCO, F. Y CALVO, J.P. 1983. Cuenca de Madrid. En: Libro Jubilar J. M. Ríos, Geología de España, II, 534-542.

LEGUEY, S., MARTÍN RUBÍ, J.A., CASAS, J. MARTA, J., CUEVAS, J., ÁLVAREZ, A. AND MEDINA J.A. 1995. Diagenetic evolution and mineral fabric in sepiolitic materials from the Vicálvaro deposit (Madrid Basin), In: G.J. Churchman, R.W. Fitzpatrick and R.A. Eggleton (Editors), *Clays: Controlling the Environment*. Proc. 10th. Clay Conf., Adelaide, Australia, 1993, CSIRO Publishing, Melbourne, Australia, p. 383-392.

LEGUEY, S., RUIZ DE LEÓN, D., RUIZ, A. I., AND CUEVAS, J. 2010. The role of biomineralization in the origin of sepiolite and dolomite. *American Journal of Science*. 310, 165-193.

MARTÍN ESCORZA, C. 1976. Actividad Tectónica durante el Mioceno en las fracturas del basamento de la fosa del Tajo. *Estudios Geológicos*. 32, 509-522.

MARTIN DE VIDALES, J. L., POZO, M., ALIA, J.M., GARACÍA-NAVARRO, F., and RULL, F. 1991. Kerolite-stevensite mixed-layers from the Madrid Basin, Central Spain. *Clay Minerals.* 26, 329-342.

MEJÍAS, A.G., ORDOÑEZ, S., Y CALVO, J.P. 1983. Nuevas aportaciones al conocimiento geológico de la Cuenca de Madrid. *Revista de Materiales y Procesos Geológicos.* 1, 163-191.

PORTERO, J. M., Y AZNAR, J.M. 1984. Evolución morfotectónica y sedimentación terciarias en el Sistema Central y Cuencas Limítrofes (Duero y Tajo). *I Congreso Español de Geología.* 3, 147-153.

ORDOÑEZ, S., CALVO, J.P., GARCÍA DEL CURA, M.A., ALONSO ZARZA AND HOYOS, M. 1991. Sedimentology of sodium sulfate and special clays from de Tertiary Madrid Basin (Spain). *Spec. Publs. Int. Ass. Sediments.* 13, 39-55.

POZO, M., CUEVAS, J., MORENO, A., REDONDO, R. Y LEGUEY, S. 1991. Caracterización de arcillas magnésicas bentoníticas en la zona de Yuncos (Toledo). *Boletín Geológico y Minero.* 102-6, 893-904.

POZO, M. AND CASAS, J. 1992. Mineralogía y sedimentología del yacimiento de saponita de Yuncos (Toledo). *Estudios Geológicos.* 48, 47-65.

POZO, M. AND CASAS, J., 1995. Distribución y caracterización de litofacies en el yacimiento de arcillas magnésicas de Esquivias (Neógeno de la Cuenca de Madrid), *Boletín Geológico y Minero.* 106, 265-282

POZO, M. and CASAS, J. 1999. Origin of kerolite and associated Mg clays in palustrine-lacustrine environments. The Esquivias deposit (Neogene Madrid Basin, Spain). *Clay Minerals.* 34, 395-418.

POZO, M., CASAS, J., MARTÍN DE VIDALES, J. L. MEDINA, J.A., y MARTÍN RUBÍ J.A. 1999. Características texturales y composicionales en depósitos de arcillas magnésicas de la Cuenca de Madrid. I) Kerolitas (sector de Esquivias y Pinto). Boletín geológico y Minero, 110-1. 77-102.

RAMIREZ, S., GARRALÓN, A., CUEVAS, J., MARTÍN-RUBÍ, J.A., CASAS, J., ÁLVAREZ, A., Y LEGUEY, S. 1996. Características químicas y propiedades de superficie en secuencia tipo de materiales esmectíticos en el yacimiento de sepiolita de Vicálvaro (Madrid). Boletín de la Sociedad Española de Mineralogía, 53-70.

RUIZ, A.I. 2010. Vicálvaro Sepiolite refinement by means of the Rietveld method (Unpublished).

TORRES, T., JUNCO, F., ZAPATA DE LA VEGA, S.L. Y PLAZA, J.M. 1984. Similitud de los procesos sedimentarios del Neogeno de la cuenca del Tajo y en la Depresión intermedia. I Congreso Español de Geología. 1, 285-300.

WRIGHT, V.E., ALONSO ZARZA, A.M., SANZ, M.E., AND CALVO, J.P. 1997. Diagenesis of Late Miocene micritic lacustrine carbonates, Madrid Basin, Spain. Sedimentary Geology.114, 81-95.

FIELD TRIP STOPS

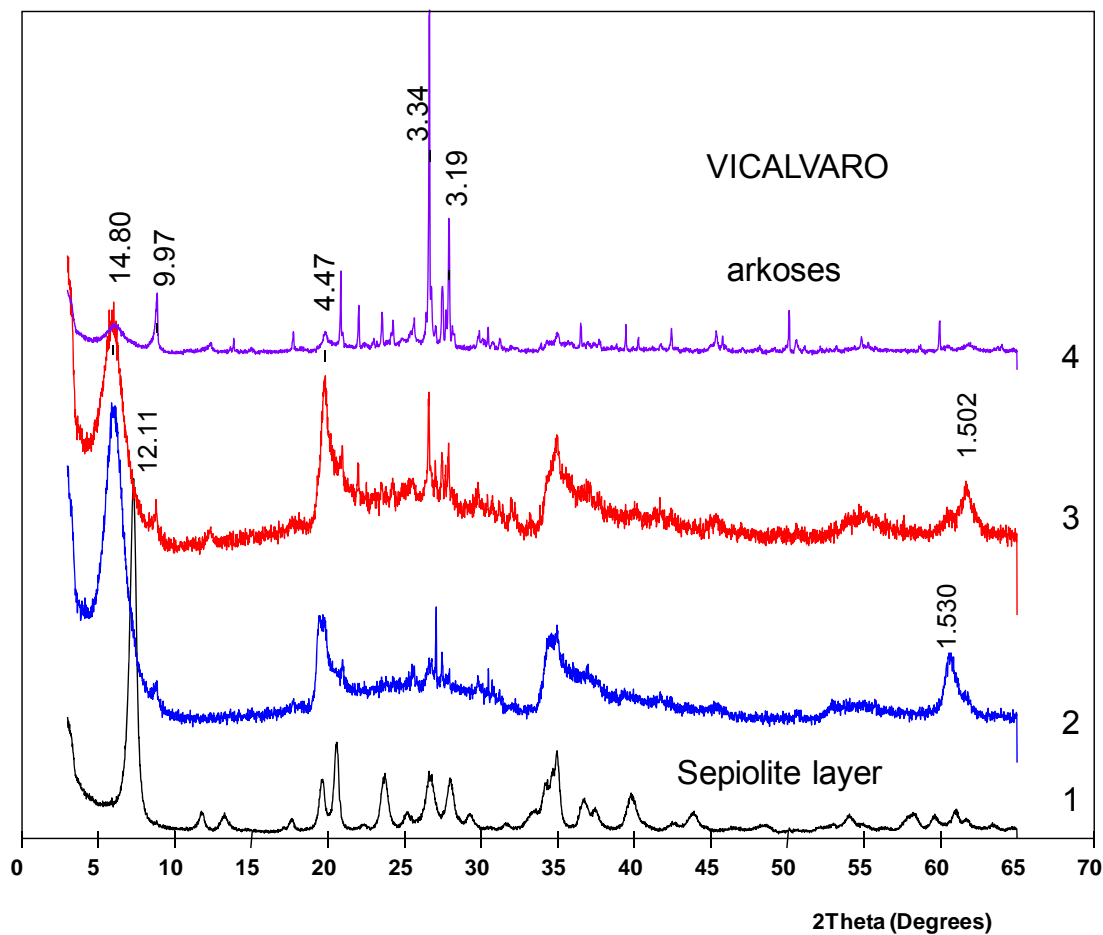
Stop 1 Vicálvaro



General view of the Vicálvaro quarry. (1): sepiolite layer; (2,3,4): transition from sepiolite to arkosic upper levels.



Detail of the exploited sepiolite layer (1) in the photograph above



X-Ray powder diffraction patterns (randomly oriented mounts) form the samples referenced in the Vicálvaro quarry photographs. Spacings (d) are expressed in Å.

The lacustrine event is buried by detrital arkosic sediments. The transition to these sediments is characterized by the presence of smectitic lutites, which evolved from trioctahedral to dioctahedral character upwards in the sequence.

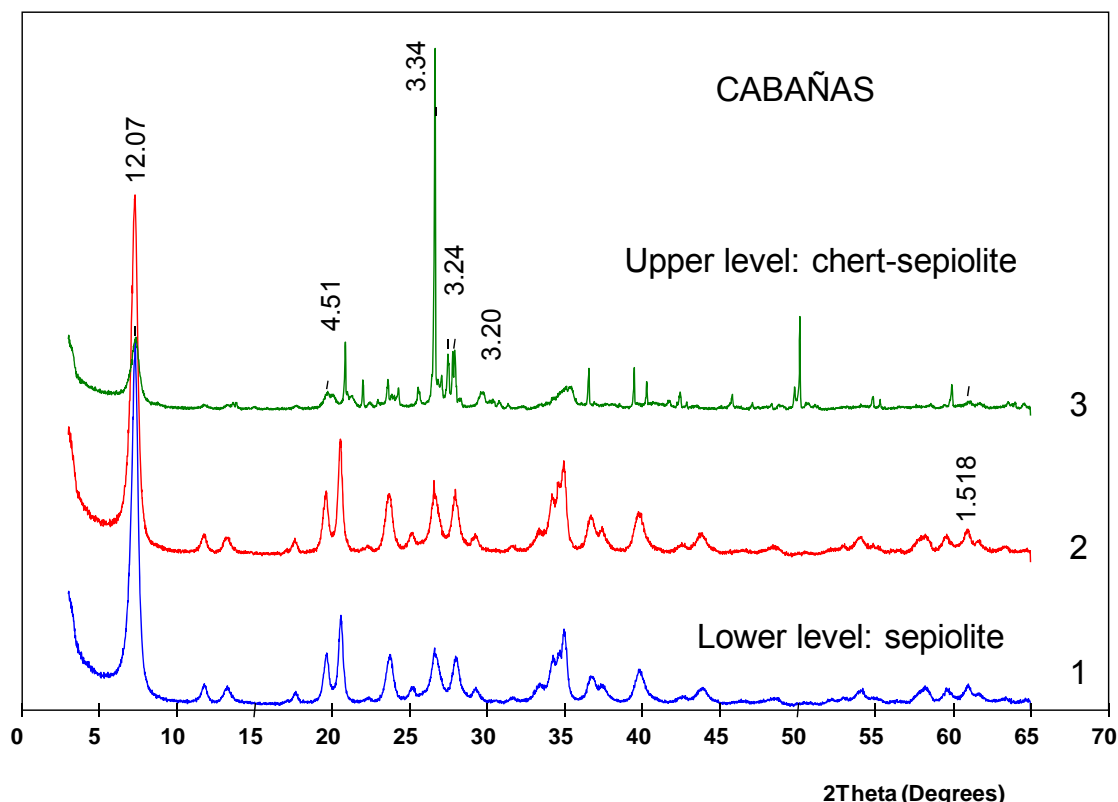
Stop 2 Cabañas de la Sagra



View of the Cabañas quarry. Upper sepiolite layer. (2): Sepiolite layer;
(3): Sepiolite with chert nodules.



Lower sepiolite layer in the Cabañas quarry. (1): Sepiolite layer



X-Ray powder diffraction patterns (randomly oriented mounts) form the samples referenced in the Cabañas quarry photographs. Spacings (d) are expressed in Å.

The Cabañas quarry offers a good chance to observe the presence of two lacustrine events separated by clastic sediments (fine grained sands). The upper sepiolite layer is seen at the top of the wet (dark brown fringes) sandy sediments located above of the lower sepiolite layer.

A discontinuous level made of chert lenses lies at the top of the upper sepiolite layer. This chert is composed of quartz. In fact, in this sepiolite layer is common to find millimeter to centimeter size nodules.

ABSTRACTS OF SYMPOSIUM LECTURES

KEYNOTE

INTRODUCTORY LECTURE

E. Galán

Departamento de Cristalografía, Mineralogía y Química Agrícola. Universidad de Sevilla, 41012 Sevilla, Spain. e.galan@us.es

Sepiolite is an uncommon mineral in spite of Si and Mg, the basic compositional cations, are two of the most abundant elements in the Earth Crust. Therefore, the genesis of sepiolite probably needs environmental conditions difficult to meet in Nature, or probably sepiolite is a very unstable mineral under supergene conditions, others than those in which the mineral was formed. In any case, sepiolite occurrences are not very frequent and commercial deposits are rare. Nevertheless, this mineral has called the attention of many clay mineralogists because of its particular structure, properties and genesis.

The main sepiolite deposits are in Spain and they account for a total production of more than 800,000 t/y. The most important deposits are located in the Tagus Basin (Madrid and Toledo) and the Ebro Basin (Zaragoza). Perhaps because of its abundance in Spain, sepiolite has been named the "Spanish Industrial Mineral". Also the most abundant referenced scientific literature corresponds to Spanish authors (more than 50%).

In this Clay Meeting twenty papers on sepiolite have been submitted, about 10% of the total papers presented, probably because of the attention given to this mineral by the organizers of the Meeting. This Symposium on sepiolite consists of a Field-Trip to the Madrid basin to visit sepiolite and other Mg-clays deposits, and a session of Invited Lectures. The first one is a General Lecture delivered by Blair Jones, which will review the Genesis and Geochemistry of Sepiolite (Blair Jones and Kathryn Conko, US Geological Survey). It will be followed by four talks, which deal with the Structure and Composition (Mercedes Suárez, University of Salamanca), the Traditional and New Applications (Antonio Álvarez, Tolsa, S.A.) and Advanced Applications (Eduardo Ruiz-Hitzky, Materials Science Institute of Madrid), and a particular approach on the Biogenic Origin of Sepiolite (Jaime Cuevas and Santiago Leguey, Autonomous University of Madrid).

I would like to remind here to Prof. Arieh Singer, one of the most outstanding researchers on Fibrous Clay Minerals, who unfortunately today is missing. He expressed me the intention to participate in this meeting. As some of you know, two years ago we decided to prepare a revision book on Palygorskite-Sepiolite. Now this book will be a tribute to Arieh Singer. The edition goes ahead, and all the invited speakers to this Symposium, join to others, (in total more than forty authors) will contribute to the book. We attempt to present in twenty chapters the most relevant aspects of these clay minerals: structure, crystal chemistry,

applications, genesis and geochemistry in different environments, occurrences and new deposits, general reviews from China, Turkey and Iran, medical and archaeological uses, etc.

I hope this Symposium on sepiolite, organized in the frame of the Trilateral Meeting on Clays will contribute to a better understanding of the genesis and particular properties of this mineral.

THE NATURAL GEOCHEMISTRY OF SEPIOLITE: A REVIEW

B. F. Jones and K. M. Conko

United States Geological Survey, 430 National Center, Reston, VA 20192, USA.
bfjones@usgs.gov

Sepiolite is most directly described as a hydrous magnesium silicate and is commonly monomineralic. The crystal structure is fundamentally a tetrahedral sheet-type, but the octahedra are discontinuous, allowing space for sorbed water, and the mineral is typically characterized as a “chain structure”. The elemental composition is an idealized $Mg_2Si_3O_7(OH)$.

The four major influences on the occurrences of sepiolite are:

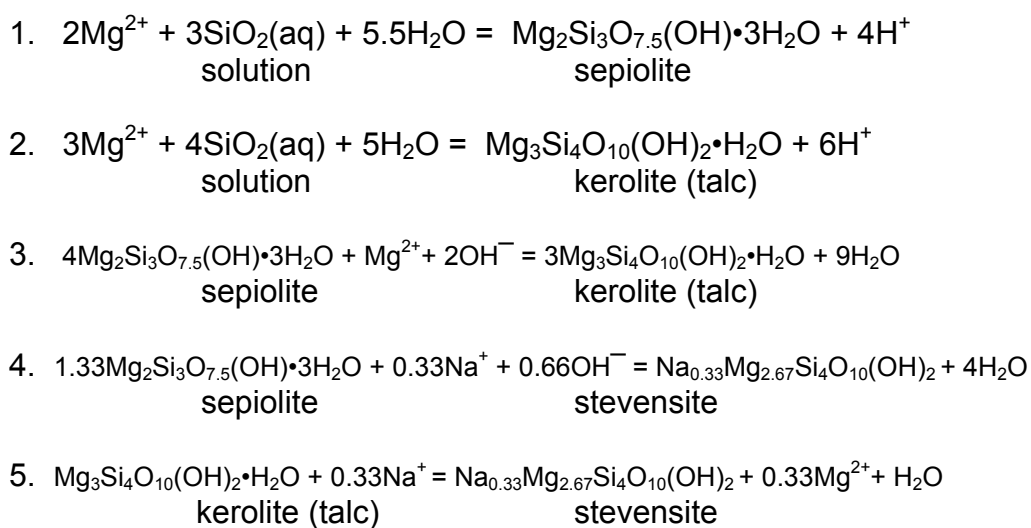
- 1) Source material: The sources of sepiolite appear to require solutions providing ionic Mg and SiO_2 in proportion of 2:3 to the near exclusion of other constituents. Solute sources include granitics to ultramafics, detrital (including colloidal), and/or dissolved, vadose and/or lacustrine sediment.
- 2) Climate: An arid to semi-arid climate, with rainfall amounts restricted depending on the regional temperature (mild to hot). In the late Tertiary, deposits are roughly concentrated at 20° to 40° north latitude and 10° to 35° south latitude (Callen, 1984).
- 3) Physical parameters: The pH range for deposition is approximately from 8 to 9. Most common substitutions are Al or Fe^{+3} in tetrahedra, divalent metal in octahedral.
- 4) Associated phases and Mg:Si ratios: Sepiolite itself (2:3), palygorskite (1:2 to 1:5), kerolite (3:4), Mg-smectite (saponite, 2:3, stevensite, 1:2), carbonates (most commonly dolomite, but can include calcite or magnesite).

There are two major mechanisms or principal controls on the occurrence and distribution of sepiolite and palygorskite; direct precipitation from solution, and the transformation of precursor phases by dissolution-precipitation. Sepiolite is most commonly found as a result of the former, whereas palygorskite is often characterized as a product of the latter. Thus, sepiolite is typically associated with lacustrine, often somewhat saline, strata, while palygorskite most commonly is the chain-structure clay phase to be found in conjunction with soils, alluvium, or most abundantly, calcretes.

Millot (1964) in his early work in North Africa presented the classic chemical scheme for closed basin clay distribution. The most aluminous and iron-rich phases are at the periphery and are succeeded basin-ward by more siliceous and magnesian clays, with sepiolite in the central area. However, the formation of sepiolite near basin center is not common, but it is more likely to be found in lacustrine-sediment transition facies leading to evaporite. Crystalline

rocks of bordering ranges are the major source of detritus and soluble silica, whereas fluctuating brackish to saline waters are the primary contributors of Mg. The most effective environment for the production of sepiolite, particularly containing a low concentration of impurities, appears to be associated with somewhat saline groundwater discharging under semi-arid climatic conditions. Probably the best examples of such conditions are the Amboseli springs of Kenya and the Amargosa desert of Nevada, USA.

Stability reactions for sesquioxide-free hydrous magnesium silicates



References

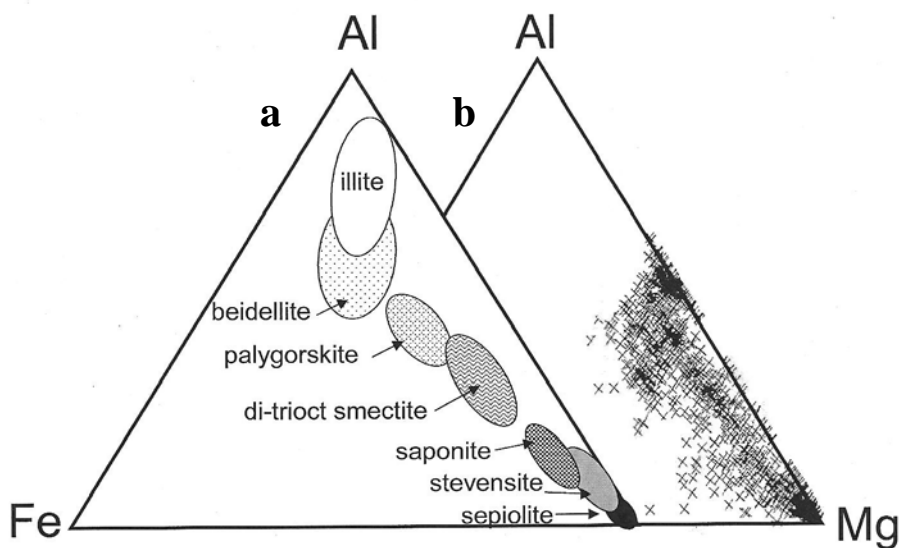
- Callen, R.A. 1984. Clays of the palygorskite-sepiolite group: Depositional environment, age and distribution. In; A. Singer and E. Galan, eds, Palygorskite-Sepiolite, Occurrences, Genesis and Uses. Developments in Sedimentology 37, Elsevier, Amsterdam, 1-37.

García-Romero E., Suárez M. 2010. On the chemical composition of sepiolite and palygorskite. *Clays and Clay Minerals*, 58(1) 1-20.

Mayayo, M. J., Torres-Ruiz, J., González-López, J.M., López-Galindo, A., Bauluz, B. 1998. Mineralogical and chemical characterization of the sepiolite/Mg-smectite deposit at Mara (Calatayud basin, Spain). *European Journal of Mineralogy*. 10, 367-383.

Millot, G. 1964. *Geologie de argiles*. Masson and Cie, Paris, 510 p.

- a) Principal octahedral cation compositions of idealized 2:1 clay mineral types from the Mara Basin of NE Spain (Mayayo et al., 1998).
- b) A world-wide suite of TEM analyzed samples of sepiolite and palygorskite (Garcia-Romero and Suarez, 2010).



STRUCTURE AND COMPOSITION OF SEPIOLITE

Mercedes Suárez

Área de Cristalografía y Mineralogía. Departamento de Geología.
Universidad de Salamanca. Plaza de la Merced s/n, 37008 Salamanca,
Spain. msuarez@usal.es

Emilia García-Romero

Departamento de Cristalografía y Mineralogía. Facultad de Ciencias
Geológicas. Universidad Complutense de Madrid. Spain. e-mail:
mromero@geo.ucm.es

Manuel Sánchez del Rio

European Synchrotron Radiation Facility. Grenoble CEDEX. France.
srio@esrf.eu

The knowledge about the structure and chemical composition of sepiolite comes from the first half of the 20th century. As it is well known, sepiolite is a fibrous clay mineral which differs from laminar clays by featuring channels in its structure. This is the result of the inversion of the apical oxygens in the tetrahedral sheets every 8 octahedral positions (or three silica chains) giving channels or tunnels with cross section of about $4 \times 11 \text{ \AA}^2$. These channels can hold zeolitic water and other molecules. Although the structure of sepiolite is well known and a crystallographic model is commonly accepted for ideal sepiolite, some natural samples of sepiolite separate from this theoretical model. Composition and structure of sepiolite vary as a function of the origin, due to different formation conditions such as temperature, pressure, chemical environment, etc. The possible variations of the structure and the chemical composition of natural sepiolites from the ideal ones (which correspond to pure and "perfect" mineral without any type of isomorphic substitution) are summarized below.

The first crystallographic model for sepiolite was proposed by Nagy and Bradley (1955). Later, Brauner and Preisinger (1956) and then Preisinger (1959) proposed a orthorhombic model with space group *Pnan* which is fully accepted by most authors. Study by AFM allow us to obtain images of individual crystals where the crystalline morphology is observed (Figure 1-a).

Sepiolite, and all clays, usually presents a fine-grained and poorly crystalline nature, therefore many details of the crystallographic structure are still not well known. Macroscopic sepiolite, millimetres in length but nanometres in section (Figure 1-b), It is not greater enough to be able to obtain diffraction pattern of single-crystal. Two-dimensional diffraction patterns have been recorded for macroscopic sepiolites using a microbeam impinging on a small bunch of sepiolite fibers (Figure 1-c). The pattern shows the lack of cylindrical symmetry

characteristic of fiber diffraction, opening a new path to study of this clay by single-crystal diffraction.

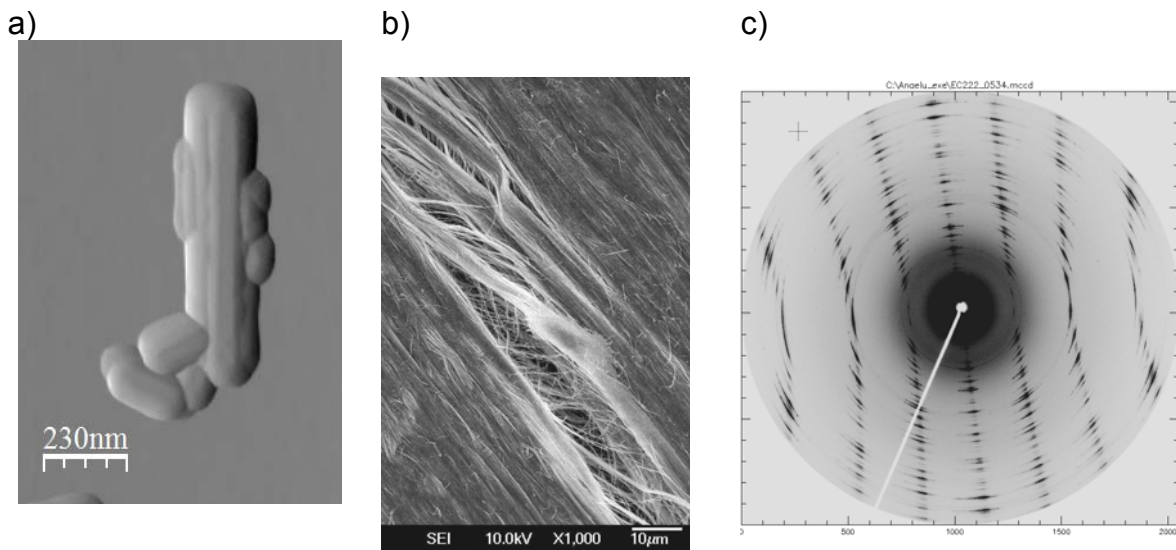


Figure 1. a) AFM image of sepiolite from Grant County (U.S.). b) SEM image of macroscopic sepiolite from Henan (China). c) 2D diffraction pattern for sepiolite from Norway obtained by using synchrotron microbeam on a bundle of parallel fibres.

Rietveld analysis is not frequently used for clay studies, because of the crystal complexity, low crystallinity and small particle size. Moreover, most authors agree with the crystallographic structure, but the fact that different sepiolites present different cell parameters, and the inexistence of sepiolite monocrystals for single-crystal diffraction, may explain why there are no crystallographic refinements of the sepiolite structure until nowadays (Post et al. 2007). Recently we have found a modification of the cell parameters as a function of the octahedral occupation and nature of the substituted cations studying a large set of sepiolite samples by synchrotron X-ray and AEM.

The ideal structural formula accepted for sepiolite based on the model of Brauner and Pressinger (1956) is: $(\text{Mg}_{8-y-z}\text{R}_y^{3+}\square_z)(\text{Si}_{12-x}\text{R}_x^{3+})\text{O}_{30}(\text{OH})_4(\text{OH}_2)_4\text{R}^{2+}_{(x-y+2z)/2}(\text{H}_2\text{O})_8$, in which the number of octahedral cations lies between 6.95 and 8.11. The octahedral cations are mainly Mg with some Al, Fe³⁺, Fe²⁺, Ti and occasional Cr³⁺ and Ni. Mg varies between 4.96 and 8.1 and $(\text{R}^2 + \text{R}^3)$ from 0 to 2.28. Recently Fe-rich sepiolites (Arranz et al. 2008) and Al-rich sepiolites (García-Romero et al. 2007) have been reported. The range and type of isomorphic compositions in the fibrous mineral can be obtained by analyzing published data of pure or almost pure sepiolites and palygorskites, a revision of bibliographic data of structural formulae of sepiolite can be found in García-Romero and Suárez (2010). In this last work, authors concluded that there is no compositional gap between sepiolite and palygorskite and intermediate terms exist. These intermediate minerals are Al-sepiolite and

Mg-palygorskite. The chemical composition of the intermediate terms can be so similar that there is a certain degree of *polymorphism* between Al-sepiolite and Mg-palygorskite. For compositions in the intervals of Si/Mg between 3.0-4.5 and $\text{Al}_2\text{O}_3+\text{Fe}_2\text{O}_3/\text{MgO}$ between 0.25-1 there are Al-rich sepiolites which can have similar chemical composition to Mg-rich palygorskites. The composition of Al-sepiolite and Mg-palygorskite is so similar between them, that an Al-sepiolite can be fitted as palygorskite with acceptable numbers of both position occupancy and charge balance. Figure 2-a shows HRXRD patterns recorded using synchrotron radiation of a very pure sepiolite. The chemical analysis of this sample obviously fits as a sepiolite: $(\text{Si}_{11.81}\text{Al}_{0.19})_{\text{O}_{30}}\text{Al}_{0.68}\text{Fe}^{3+}_{0.28}\text{Mg}_{6.10}(\text{OH}_2)_2(\text{OH})_4\text{Ca}_{0.18}\text{K}_{0.12}\text{Na}_{0.04}\text{4H}_2\text{O}$, but also as palygorskite $(\text{Si}_{7.87}\text{Al}_{0.13})_{\text{O}_{20}}\text{Al}_{0.41}\text{Fe}^{3+}_{0.13}\text{Mg}_{4.05}(\text{OH})_2(\text{OH}_2)_4\text{Ca}_{0.07}\text{K}_{0.05}\text{Na}_{0.05}\text{4H}_2\text{O}$. A structural model for this Al-rich sepiolite is proposed in figure 2-b in which a portion of palygorskite polysomes is intergrown with the sepiolite polysomes. The chemical analysis of this sample presents a few Al_2O_3 and the MgO content is only a bit lower than theoretical sepiolite this chemical analysis would be usually interpreted as a sepiolite with some Al substituting Mg.

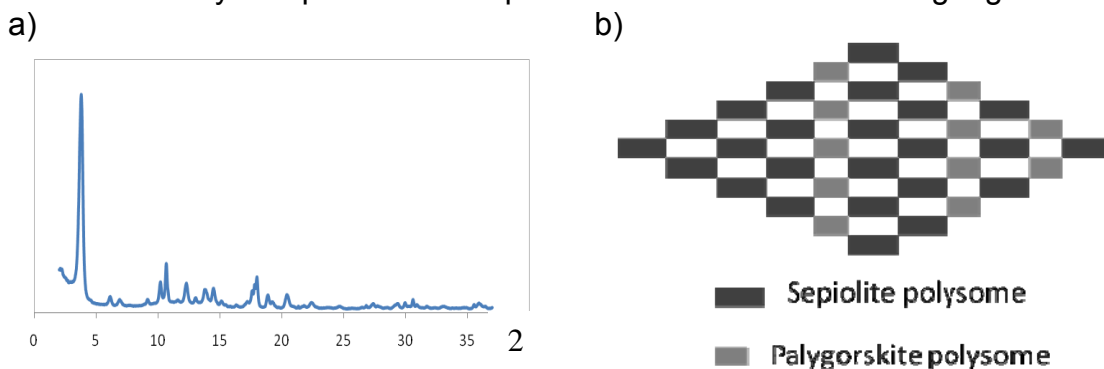


Figure 2: a) HRXRD pattern for pure sepiolite from Batallones (Madrid, Spain) recorded at $d=0.79988 \text{ \AA}$. b) Simplified structural model proposed for this sample with a mixture of sepiolite and palygorskite polysomes.

The possibility of polysomatism in sepiolite-palygorskite was referred to by Ferraris et al. (1998) and it was also suggested for palygorskite with an excess of Mg (Statopoulou et al., submitted). If the polysomatic model is taken into account, then the existence of Al-sepiolite could also be explained with the presence of palygorskite polysomes in the sepiolite structure. It is feasible to wonder about the existence of all possibilities in the continuous series, from the purest and the most exclusive magnesian sepiolite, to the purest palygorskite, with all intermediate compositions. These compositions include palygorskite with different portions of sepiolite polysomes, and the contrary, sepiolite with all possible portions of palygorskite polysomes.

References

- Arranz, E. and Lago, M. and Bastida, J., Galés, C., Soriano, J., and Ubide, T. 2008. Hydrothermal macroscopic Fe-sepiolite from Oujda mounts (Middle Atlas, Eastern Morocco). *Journal of African Earth Science*, 52, 3, 81-88.
- Brauner, K. and Pressinger, A. 1956. Struktur und Entstehung des Sepioliths. *Tschermak's Mineralogische und Petrographische Mitteilungen*, 6, 120-140.
- Ferraris, G., Khomyakov, A. P., Belluso, and E., Soboleva, S.V. 1998. Kalifersite, a new alkaline silicate from Kola Peninsula (Russia), based on a palygorskite-sepiolite polysomatic series. *European Journal of Mineralogy*. 10, 865-874.
- García-Romero, E.; Suárez, M.; Santaren, J. and Alvarez, A. (2007) Crystallochemical characterization of the palygorskite and sepiolite from the Allou Kagne deposit. *Senegal. Clays and Clay Minerals*. 6, 606-617.
- García-Romero, E. and Suárez, M. 2010. On the chemical composition of sepiolite and palygorskite. *Clays and Clay Minerals*. 58, 1-20.
- Nagy, B. and Bradley, W.F. 1955. The structural scheme of sepiolite. *American Mineralogist*. 40, 885-892.
- Post, J.E., Bish, D.L., and Heaney, P.J. 2007. 'Synchrotron powder X-ray diffraction study of the structure and dehydration behavior of sepiolite'. *American Mineralogist*. 92, 91-97.
- Preisinger, A. 1959. X-ray study of the structure of sepiolite. *Clays and Clay Minerals*, 6, 61-67.
- Statopoulou, E.T., Suárez, M., García-Romero, E., Sánchez del Rio, M., Kacandes, G., Gionis, V. and Kryssikos, G.D.(submitted). Trioctahedral entities in palygorskite: A case of polysomatism?. *American Mineralogist*.

EVIDENCES FOR BIOGENIC ORIGIN OF SEPIOLITE

S. Leguey, and J. Cuevas

Departamento de Geología y Geoquímica, Facultad de Ciencias. Universidad Autónoma de Madrid. Cantoblanco s/n. 28049 Madrid, Spain.

jaime.cuevas@uam.es

The formation of different authigenic minerals as dolomite, magnesite, barite, Fe-oxides, pyrite and chert has been described in the lacustrine and fluvio-lacustrine Miocene sediments of the Madrid basin. Several mineralogical, textural and geochemical data put some evidence on the role of the microorganisms activity in their formation (Sanz Montero et al., 2008; 2009). Leguey et al., 2010, have found also indirect evidences of sepiolite formation by biogenic related mechanisms in dolomite-sepiolite materials formed in shallow lacustrine environments from the intermediate unit of the Miocene in the NE area of the Madrid Basin. These sediments contain dolomite aggregates reminiscent of mineralized microorganisms with ovoid morphologies and spherical to tubular voids (termed biomorphs). Also, fibrous sepiolite-dolomite intergrowths have been frequently observed closely related to these biomorphs.

Sepiolite and palygorskite have been found in geological environments where microbiological activity is presumed. This fact is supported by several morphological and biogeochemical signatures. Some examples are the observation of rosary-like chain of beads forming palygorskite or filamentous and tubular forms of silica (Folk and Rasbury, 2007, Leguey et al., 2010); the precipitation of sepiolite by reaction of Mg ions in seawater with biogenic silica (Yan and others, 2005); or the sepiolite filled boxwork textures in coccolith laminated aggregates, found in mid-ocean ridge environments (Hathaway and Sachs, 1965).

Crystalline Mg-silicate mineral phases are rarely mentioned related to cyanobacteria microbial mats and benthic communities in saline alkaline wetlands. However, Mg-silicate layers and amorphous coatings are present in carbonate microbialites (Arp et al., 2003) or in association to extracellular polymeric substances (EPS) during the fossilization of green algae and cyanobacteria cell walls (Souza-Egipsy and others, 2005; Pacton and others, 2009). Moreover, Mg and Si solution concentration drops dramatically during Mg-carbonates biologically induced mineralization (Power and others, 2007). As a conclusion, some of these authors suggested the presence of this Si-Mg coatings, within carbonate precipitates, to be a signature for microbiological activity.

In the case of the dolomite-sepiolite sediments from the Madrid basin, a group of evidences has been collected in order to support their biogenic origin:

- K (microcline, illite, biotite) relative depletion in sediments with sepiolite (solubilized as nutrient?).
- gypsum/dolomite and reducing interfaces (sulphides, Organic matter) in basal sediments preceding sepiolite (SRB bacteria ?)
- Biomorphs: silica rosary chains, dolomite and mixtures of dolomite-sepiolite ovoids (dumbbells)
- Regular size and shape of biomorphs with submicron platy dolomite crystals (BET surface of dolomite: 20-30 m²/g) with internal cellular texture.
- Size of individual crystals and internal macropores compatible with microorganisms (< 2 µm)
- Light source for carbon in dolomite associated to sepiolite: $\delta^{13}\text{C} < 7\text{\textperthousand}$
- Determination of permil amounts of nC<18 fatty acid compounds extracted in metanol (biomarkers for algae and bacteria in the lacustrine environment).

As a first approach to search for a biogenic origin of sepiolite, our aim have been to analyze the geochemical and textural characteristics of the mineralized biomass found in the sediments. Hydration-desiccation cycles occur in the sediments and favor the biomass degradation and the dissolution-precipitation processes. In this environment, the sepiolite and/or dolomite or the opal are concentrated. Investigation tools such as scanning and transmission electron microscopy have allowed us, at micro and nanometer scale, to evidence how the mineralization of biomass is the driving process of mineral formation.

The proposed biomineralization process occur in two steps. In the first step, the passive biomineralization on EPS (Si, Ca and Mg) adhered to vegetal remains is produced, and silica is found as nanotubes (Fig. 1). In the second stage, the Mg, previously concentrated on EPS generated by microorganisms (i.e., cyanobacteria) or mineralized as dolomite, is liberated during the desiccation processes (Wright and Wacey, 2005). Reaction of Mg with the biogenic silica lead to the sepiolite crystals nucleation using the organic support (Fig. 2). When the concentration of Mg is low or when the organic support is scarce, biogenic silica predominates and is later transformed (aged) into quartz. Diagenetic processes favor the more soluble precipitated salts and organic matter loss and the growing of the sepiolite fibers, which preserve the structure of microfibers and intergrowths of preexistant nanotubes.

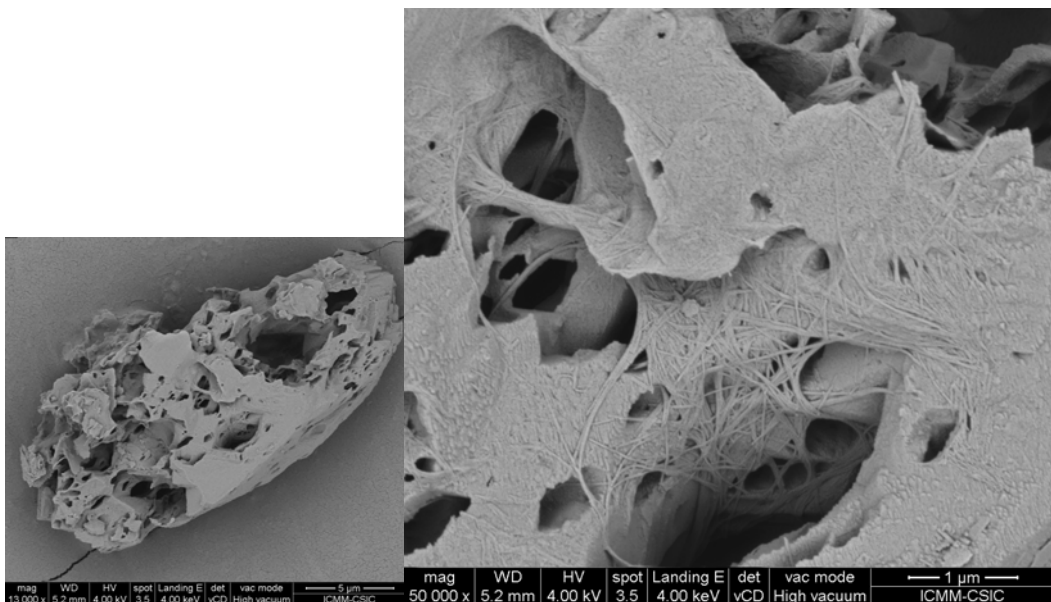


Fig.1: dolomite biomorph (left) integrated with silica nanotubes (detail, right)

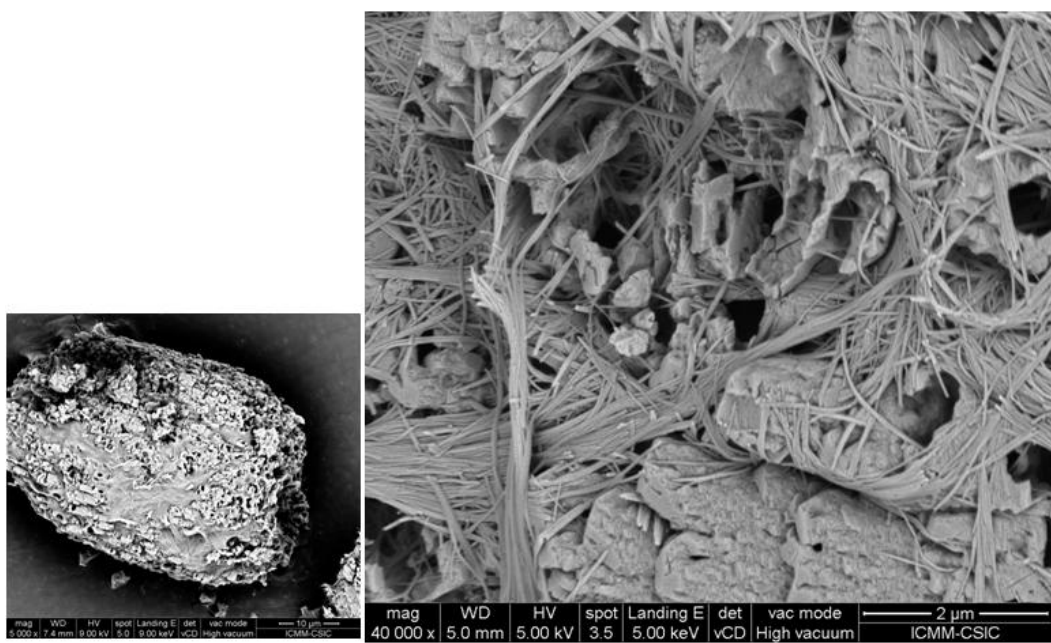


Fig. 2: sepiolite biomorph with residual cellular dolomite. Detail (right)

References

- Arp, G., Reimer, A. and Reitner, J. 2003. Microbialite Formation in Seawater of Increased Alkalinity, Satonda Crater Lake, Indonesia. *Journal of Sedimentary Research.* 73. 105-127.

Folk, R.L. and Rasbury, T. 2007. Nanostructure of Palygorskite/sepiolite in Texas Caliche: Possible Bacterial Origin. *Carbonates and evaporates.* 22, 113-122.

Hathaway, J.C., and Sachs, P.L. 1965. Sepiolite And Clinoptilolite From The Mid-Atlantic Ridge. *American Mineralogist,* VOL. 50, 852-867.

Leguey, S. , Cuevas, J., Ruiz, A.I. and Ruiz León, D. 2010. The Role Of Biomineralization in the Origin of Sepiolite and Dolomite. *American Journal of Science.* 310,165–193.

Pacton, M., Ariztegui, D., Vascocellos, C., Barbarand, J., Gorin, G.E., and McKenzie, J.A. 2009. Formation of Amorphous Mg-Si Precipitates mediated by Microbial Activity: A Recent Analogue for Understanding their Role in Microbialite Formation. 2009. American Geophysical Union, Fall Meeting, abstract B21A-0319.

Power, I.M., Wilson, S.A., J.M. Thom, G.M. Dipple and G. Southam. 2007. Biologically induced mineralization of dypingite by cyanobacteria form an alkaline wetland near Atlin, British Columbia, Canada. *Geochemical transactions.* 8, 13.

Sanz-Montero, M.E. y Rodríguez-Aranda J.P. (2008): Participación Microbiana en la Formación de Magnesita dentro de un Ambiente Lacustre Evaporítico: Mioceno de la Cuenca de Madrid. *Macia* 9, 231-232.

Sanz-Montero, M.E., Rodriguez-Aranda, J.P., Y Pérez-Soba, C. (2009): Microbial weathering of Fe-rich phyllosilicates and formation of pyrite in the dolomite precipitating environment of a Miocene lacustrine system. *European Journal Mineralogy,* 21, 163-175.

Souza-Egpsy, V., Wierzchos, J., Ascaso, C. and Nealson, K.H. 2005. Mg-silica precipitation in fossilization mechanisms of sand tufa endolithic microbial community, Mono Lake (California). *Chemical Geology.* 217, 77-87.

Wright, D. T. and Wacey, D. 2005. Dolomite precipitation in experiments using sulphate reducing bacterial populations in simulated lake and pore waters from distal ephemeral lakes, Coorong region, South Australia. *Sedimentology.* 52, 987–1008

Yan, J., Munnecke, A., Steuber, T., Carlson, E.H. and Xiao, Y., 2005, Marine sepiolite in middle Permian carbonates of south China: implications for secular variation of Phanerozoic Seawater Chemistry: *Journal of Sedimentary Research,* v. 75, p. 328-338.

SEPIOLITE: AN OVERVIEW FROM TRADITIONAL MARKETS TO NEW APPLICATIONS

A.Alvarez (Group Technological Innovation Director, Grupo Tolsa)
aalvarez@tolsa.com

The objective of this presentation is to give an overview of the application and markets of products that are currently manufactured with this mineral, as well as the new applications that are being developed and which are expected to become a reality in the near future.

We will review the different generations of products that can be obtained with this mineral by using different industrial processes. When Robertson and Chambers described the potential industrial applications of this unusual mineral more than fifty years ago, many of the applications were more a possibility based on the peculiar properties of sepiolite than a reality at that time. However, since then, sepiolite has proved to be a very versatile raw material and a significant work of development has resulted in a whole range of sepiolite-based products. In this sense, we can differentiate the following generations of products produced from sepiolite:

- Products obtained by conventional crushing and grinding, such as industrial absorbents or cat litter. These products are mainly used on the sorption properties of sepiolite.
- Products obtained by micronization processes, including dry and wet micronization processes, which are used as fillers and rheological additives for different applications from rubber to coatings. Sepiolite is used in many of these applications to modify the rheological characteristics of the systems thanks to the adsorption properties of the clay and the high aspect ratio of the needle-like sepiolite particles
- Products obtained by surface modification of sepiolite, which allow modify the hydrophilicity of the sepiolite surface and use this clay in organic systems as greases or solvent-based paints.
- Products obtained by combination of sepiolite with different additives in order to enhance some absorption characteristics or rheological properties of sepiolite. Some of these products are used as rheology modifiers for building materials.
- Products obtained by chemical treatment of sepiolite in order to enhance certain properties as surface area or cation exchange capacity. Thus, it is possible obtain special fibrous silicas with high surface area or synthetic loughlinites with high CEC that can be exchanged with aluminium to increase the surface acidity in order to obtain additives for FCC.

- Nanomaterials and new functional materials obtained from sepiolite. Sepiolite-based nanoclays can be used as nanofillers for polymers in order to enhance mechanical and thermal properties, and improve fire retardancy behaviour. Furthermore, new sepiolite-based nanomaterials functionalized with different metal nanoparticles or nanooxides can be obtained with new and improved properties.

The new developments carried out with this mineral show that the versatility of sepiolite still offers opportunities to face the challenges of the future. These challenges have been addressed by the WBCSD Vision for 2050, that is, the result of the collaborative effort of leading companies committed to sustainable development through economic growth, ecological balance and social progress. The objective of this report is to show the pathway to connect the present with a future when in 2050 around 9 billion people could live well, and within the limits of the planet. A key element in this pathway is the development of new materials which could permit to make more with less. The new materials should be able to deliver more functionalities, last longer and be designed to be reused or recycled. These materials should allow meet the objectives of more energy efficient products such as lighter materials for cars or energy efficient buildings. The new materials that are being developed from sepiolite, including nanomaterials, functional hybrid materials or bio-inspired and biomimetic materials show the possibilities to obtain materials that can meet the requirements to get the objectives of the 2050 Vision, in different areas as buildings, mobility, energy, or agriculture. The eco-efficient use, reuse and recycling of minerals as sepiolite that are non-renewable resources are also a challenge to solve.

1. Chambers, P.C. (1959) Some industrial applications of the clay mineral sepiolite. *Silicates Industriels*, 24, 181
2. Robertson R.H.S. (1957) Sepiolite: A versatile raw material. *Chem. Ind.*, 1492-1495
3. Alvarez, A. (1984). Sepiolite: properties and uses. Chapter in Palygorskite and Sepiolite Occurrences, Genesis and Uses. *Developments in Sedimentology*, Vol. 37, 253-287, Eds. Singer, A. and Galan, E.
4. Galan, E. (1996) Properties and Applications of Sepiolite-Palygorskite clays. *Clay Minerals*, 31, 443-453
5. Pecharromán C., Esteban-Cubillo A., Montero I. and Moya J. S. (2006) Monodisperse and Corrosion-Resistant Metallic Nanoparticles Embedded into Sepiolite Particles for Optical and Magnetic Applications *J. Am. Ceram. Soc.* 89 3043–9
6. Vision 2050. The new agenda for business. Worl Business Council for Sustainable Development (2010)

SEPIOLITE: A SINGULAR CLAY FOR ADVANCED APPLICATIONS

E. Ruiz-Hitzky

Instituto de Ciencia de Materiales de Madrid, CSIC. Cantoblanco, 28049
Madrid, Spain eduardo@icmm.csic.es

Since the pioneering work published several decades ago by Roberston (1) on general applications of sepiolite, few reviews regarding the relationships between structural and textural features and uses of this unique microfibrous clay and its parent mineralogical one, palygorskite, have been published (2,3)

The recent development of the so-called “sepiolite advanced materials” is mainly based on the singular structural and textural features of this silicate. In particular its surface properties, and therefore the ability to interact with many compounds, have opened the way for the preparation of a wide variety of nanostructured materials derived from sepiolite. In the present communication we intend to introduce some results on this type of sepiolite-based materials with particular emphasis to those obtained in our group.

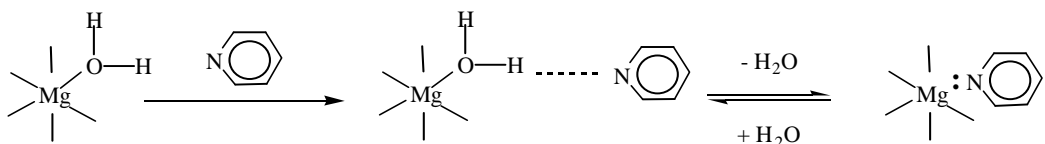
It is well known that sepiolite exhibits particular textural properties such as an elevated specific surface area and a hierarchical distribution of pores. These characteristics represent singular surface behaviors that are determinant for current and future applications of sepiolite. We will introduce in the first part of this communication diverse applications due to the presence of nanopores determining the internal surface of sepiolite, and in a second part we will specially consider modifications of the external surface of this silicate.

The intracrystalline cavities (*tunnels*) with a section of ca. $1 \times 0.5 \text{ nm}^2$ can be considered as nanopores that can be accessible to appropriate molecular species (4,5). The Howarth-Kawazoe analysis of sepiolite from the Ar adsorption isotherms, shows a predominance of about 0.65 nm diameter pores, which is in good accordance with the nanopore dimensions deduced from the sepiolite crystal structure (6).

Sepiolite –as well as palygorskite- can act as a molecular sieve discriminating the uptake of species by its molecular size (5,7). Intracrystalline adsorption is also favored by the polar character of the molecules being able to penetrate into the tunnels, as occurs for instance with ammonia, methanol, ethanol, acetone, ethylene glycol and pyridine (5,9).

Interaction mechanisms between the internal surface and the molecular adsorbates can be diverse: H-bonding, co-ordination and ion-exchange. Water molecules coordinated to Mg^{2+} ions at the border of the ribbons inside the tunnels could participate in hydrogen bonding, water bridges and even in the $\text{H}_2\text{O}-\text{Mg}$ direct coordination with small polar molecules. This is for example, the case of pyridine that can be sequestered into the sepiolite tunnels by direct coordination to Mg^{2+} when the samples are thermally treated (Scheme 1) (10).

Scheme 1. Direct coordination of pyridine to Mg^{2+} by replacing the coordinated water molecules in sepiolite.



Cationic species with appropriate molecular dimensions, such as the methylene blue, acridine orange and thioflavine-T cationic dyes, penetrates inside these nanopores (11-13). Methylene blue has compatible dimensions ($1.7 \times 0.76 \times 0.32 \text{ nm}^3$) to penetrate into the structural tunnels, but due to its tendency to increase its dimensions by forming voluminous molecular aggregates is impeded to accede into the nanopores from concentrated solutions. It can be only adsorbed there from diluted solutions ($<10^{-3} \text{ M}$), *i.e.* when it is present in monomeric form (5). In the case of acridine orange, it has been shown the highly specific directional binding of the dye into sepiolite, the molecules being arranged with their long axes parallel to the sepiolite fiber axis (14).

The molecular access to sepiolite tunnels that explains the salient stability of indigo (ancient Maya Blue) (15-18) adsorbed on the silicate is of interest for the development of Maya-Blue based materials in formulations for high performance outdoors paints (19,20). On the other hand, the Michler's hydrol is an indicator that changes its color in the presence of thiols (mercaptanes), which are responsible of unpleasant odors, producing colorless adducts. The adsorption of this dye on sepiolite allows to easily detect thiols originated from industrial waste, wastewater treatments, halitosis, animal breeding and domestic animals (Fig.1) (21).

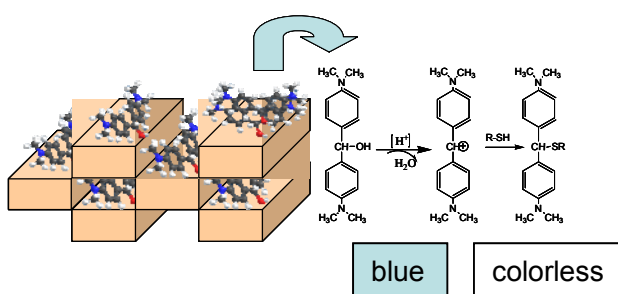


Fig. 2. Sepiolite-Michler's hydrol compounds used for thiols detection (ref. 21).

Certain monomers that can further polymerize (e.g. acrylonitrile, ref. 22) and even some specific linear polymers (e.g. polyethylene oxide, ref 5,) are also able to penetrate the nanopores giving rise to polymer-sepiolite nanocomposites. The templated polyacrylonitrile submitted to further thermal treatment can be recovered as carbon nanofibers provided with electrical conductivity that can be used as efficient electrodes in Li-batteries (22).

Other recent examples of nanostructured sepiolite derivatives prepared in our Laboratory, which mainly imply modifications of the external surface of the mineral, will be introduced in this communication to show the development of advanced materials useful for a wide type of applications, including energy storage, environmental and biomedical fields (Table 1).

In this context, carbon-sepiolite nanocomposites can be easily prepared from cheap, abundant and non-toxic precursors such as sucrose (sugar table). Caramel-sepiolite nanocomposites can be further transformed into graphene-like composites provided of good electronic conductivity of interest as active elements in electrochemical devices such as sensors, batteries and supercapacitors (23-25). Interestingly, sepiolite can be directly combined with carbon-nanotubes (CNTs) following a patented procedure (26), which provides an excellent colloidal stability to these nanotubes in aqueous dispersions. Sepiolite-CNTs *buckypapers* can be prepared by this new procedure. Surface modification by coverage of inorganic compounds such as silica and TiO₂ were developed by a sol-gel route using Si- and Ti-alkoxides as starting reagents and sepiolite modified with surfactants (27, 28). Magnetite nanoparticles included in ferrofluids can be associated to sepiolite in soft experimental conditions giving stable derivatives that show superparamagnetic properties preserving the main characteristics of sepiolite, in particular its sorption ability (29). These materials are an excellent alternative to the filtration and membrane-based procedures, being of interest for the easy removing of pollutants from water, including radioactive cationic species. They can be also used as additives of polymers conferring magnetic properties to the resulting nanocomposites that can be applied for the preparation of panels provided of shielding ability towards electromagnetic radiation. Other new type of sepiolite based nanostructured materials are LDH and zeolite heterostructures prepared by growth of small size crystals of these last solids on the external surface of the silicate (30,31). In the case of the LDH-sepiolite heterostructures a synergistic effect, such as the capacity to act as anion- and cation-exchanger material can be applied in the development of multifunctional solids (30). Homogeneous sepiolite-smectite heterostructures have been recently developed in our group by combination of both of the clay components previously modified with surfactants and coated with small amounts silica (31). Finally, biohybrids derived from sepiolite by its assembling under soft conditions with diverse biopolymers (polysaccharides, proteins, lipids and nucleic acids) (33-35) offers a wide range of potential applications from insulating incombustible foams (36) to new systems for drug delivery systems (37), including the use as support of viruses and its application as adjuvant of vaccines (38).

Table 1. Recent examples of nanostructured materials prepared from sepiolite.

Sepiolite based nanostructured materials	Preparation procedure	Properties/ Potential applications	Authors/Ref.
Graphenoids-sepiolite nanocomposites	Adsorption of sucrose as carbonaceous precursor followed of thermal treatment (caramel-sepiolite intermediates)	Good electrical conductivity, maintaining the sepiolite properties Development of electrochemical devices (sensors, batteries,...)	Gómez-Avilés et al., 2007 and 2010 (refs. 23, 24) Fernández-Saavedra et al., 2008 (ref. 25)
Carbon-nanotubes (CNTs)/sepiolite nanocomposites	Assisted assembling in aqueous media	Electronic conductivity. Very stable and high viscosity dispersions Reinforcement and functionalization of polymers. <i>Buckypaper</i> production.	Fernandes & Ruiz-Hitzky, 2009 (ref. 26)
Silica-sepiolite nanocomposites	Surface coverage from Si-alkoxides (sol-gel) of organo-sepiolites	Glass microfibers-like easy to functionalize Reinforcement of epoxy and other polymers Support of enzymes, catalysts, etc	Gómez-Avilés et al. 2010, (ref 27)
Anatase nanoparticles/sepiolite	Sol-gel of Ti-alkoxides in the presence of sepiolite modified by surfactants	High specific surface photoactive systems Photodecomposition of organic pollutants in water	Aranda et al., 2008, (ref. 28)
Magnetic nanoparticles/sepiolite	Infiltration of magnetite-based ferrofluids	Superparamagnetic behaviour maintaining the sepiolite properties Removal of organic pollutants and radionuclides from water Magnetic polymer-sepiolite nanocomposites. Panels for microwave shielding (antiradar systems)	Ruiz-Hitzky, Aranda, Gonzalez, 2010, (ref. 29)
LDH-sepiolite heterostructures	Growth of layered double hydroxides grafted on the external surface of sepiolite	Dual properties from both sepiolite and LDH: simultaneous anionic and cationic exchange ability Adsorption of pollutants and heterogeneous catalysis	Ruiz-Hitzky, Aranda & Gómez-Avilés, 2008 (ref. 30)
Zeolites-sepiolite heterostructures	Growth of nanosized zeolites on the external surface of sepiolite	Synergistic properties of zeolites and sepiolite Ion-exchangers, adsorbents of pollutants and heterogeneous catalysis	Gómez-Avilés et al. (ref. 31) (<i>in preparation</i>)
Sepiolite-Smectites heterostructures	Combination between organic derivatives of clays in the presence of silica precursors	Synergistic properties of both types of clay minerals. Polymer reinforcement	Aranda, Gómez-Avilés, Ruiz-Hitzky, 2010, (ref. 32)
Biopolymers-sepiolite nanocomposites (Bio-nanocomposites)	Assembling of polysaccharides, proteins, lipids and nucleic acids to sepiolite	Bio-nanocomposites can be conformed as powders, thin films or monolithic blocks with cellular texture. Biodegradable, biocompatible, fire retardancy, bioactivity, etc. Active phase of sensors, thermal and acoustic insulating materials, support of enzymes, adjuvant of vaccines	Darder et al., 2006 (ref. 33) Ruiz-Hitzky, Darder, Aranda, 2007 (ref. 34) Ruiz-Hitzky et al., 2009 & 2010 (refs. 35, 38, & 39)

References

- 1 R.H.S. Robertson, Chem. and Ind., 16, 1492-1495 (1957)
- 2 E. Galán, Clay Miner. 31, 443-453 (1996)
- 3 M.F. Brigatti, E Galán, BKG Theng, in: Handbook of Clay Science, F Bergaya, BKG Theng and G Lagaly, Eds., pp 56-69, Elsevier, Amsterdam, 2006.
- 4 J.M. Serratosa, in: Proc. Internat Clay Conf., Oxford, 1978, MM Mortland and VC Farmer, Eds., pp 99-109, Elsevier, Amsterdam, 1979.
- 5 E. Ruiz-Hitzky, J. Mater. Chem. 11, 86-91 (2001)
- 6 K. Brauner, Preisinger A., Miner. Petr. Mitt. 6, 120-140 (1956)
- 7 R.M. Barrer, N. Mackenzie, J. Phys. Chem. 58, 560-568 (1954)
- 8 R.M. Barrer, N. Mackenzie, D.M. MacLeod, J. Phys. Chem. 58, 568-572 (1954)

- 9 E. Ruiz-Hitzky, P. Aranda, J. M. Serratosa, in *Handbook of Layered Materials*, Chapter 3, pp. 91–154, S. M. Auerbach, K. A. Carrado and P. K. Dutta, Eds., Marcel Dekker, New York, 2004.
- 10 W. Kuang, G. A. Facey, C. Detellier, B. Casal, J. M. Serratosa, E. Ruiz-Hitzky, *Chem. Mater.* 15, 4956–4967 (2003)
- 11 Aznar J. A., Casal B., Ruiz-Hitzky E., Lopez-Arbeloa I., Lopez-Arbeloa F., Santaren J., Alvarez A., *Clay Miner.*, 27, 101 (1992)
- 12 Rytwo G., Nir S., Margulies L., Casal B., Merino J., Ruiz-Hitzky E. , Serratosa J.M., *Clays Clay Miner.*, 46, 340 (1998)
- 13 B. Casal, J. Merino, J.M. Serratosa, E. Ruiz-Hitzky, *Appl. Clay Sci.* 18, 245–254 (2001)
- 14 P.S. Ridler, B.R. Jennings, *Clay Miner.*, 15, 121–133 (1980)
- 15 M. Sánchez del Río, P. Martinetto, C. Reyes-Valerio, E. Dooryhée, M. Suárez, *Archaeometry*, 48, 115–130 (2006)
- 16 H. Berke, *Chem. Soc. Rev.*, 36, 15–30 (2007)
- 17 G. Chiari, R. Giustetto, J. Druzik, E. Doehne, G. Ricchiardi, *Appl. Phys. A*, 90, 3–7 (2008)
- 18 M. Sánchez del Río, E. Boccaleri, M. Milanesio, G. Croce, W. van Beek, C. Tsiantos, G. D. Chyssikos, V. Gionis, G.H. Kacandes, M. Suárez, E. García-Romero, *J. Mater. Sci.*, 44, 5524–5536 (2009)
- 19 F. Gándara, F. López-Arbeloa, E. Ruiz-Hitzky, M. A. Camblor, *J. Mater. Chem.*, 16, 1765–1771 (2006)
- 20 F. Gándara, K. Miyagawa, P. Aranda, E. Ruiz-Hitzky, M. A. Camblor, in *Jornada Científica Conmemorativa 50 Aniversario de la SEA*, E. Ruiz-Hitzky and P. Aranda, Eds., Madrid, 2009
- 21 Aranda, P., Salvador, R., Ruiz-Hitzky, E., Alvarez, A., Duch, de Juan, F., Sp. Patent 200402189 (2004)
- 22 R. Fernandez-Saavedra, P. Aranda, E. Ruiz-Hitzky, *Adv. Funct. Mater.* 14, 77–82 (2004)
- 23 A. Gómez-Avilés, M. Darder, P. Aranda, E. Ruiz-Hitzky, *Angew. Chem.* 46, 923–925 (2007)
- 24 A. Gómez-Avilés, M. Darder, P. Aranda, E. Ruiz-Hitzky, *Appl. Clay Sci.*, DOI: 10.1016/j.clay.2009.10.004 (2010)
- 25 R. Fernández-Saavedra, M. Darder, A. Gómez-Avilés, P. Aranda, E. Ruiz-Hitzky, *J. Nanosci. Nanotech.* 8, 1741–1750 (2008)
- 26 F.M. Fernandes, E. Ruiz-Hitzky, Sp. Patent 200931135 (2009)
- 27 A. Gómez-Avilés, F. M. Fernández, E. Ruiz-Pachón, E. Ruiz-Hitzky, *in preparation* (2010).
- 28 P. Aranda, R. Kun, M.A. Martín-Luengo, S. Letaïef, I. Dékány, E. Ruiz-Hitzky, *Chem. Mater.* 20, 84–89 (2008)
- 29 E. Ruiz-Hitzky, P. Aranda, Y. Gonzalez, Sp. Patent 201030333 (2010)
- 30 E. Ruiz-Hitzky, P. Aranda, A. Gómez-Avilés, Sp. Patent 200803642, PCT/ES2009/070535 (2008)
- 31 A. Gómez-Avilés, M.A. Camblor, P. Aranda, E. Ruiz-Hitzky, *in preparation* (2010)
- 32 P. Aranda, A. Gómez-Avilés, E. Ruiz-Hitzky, *in preparation* (2010)
- 33 M. Darder, M. López-Blanco, P. Aranda, A.J. Aznar, J. Bravo, E. Ruiz-Hitzky, *Chem. Mater.*, 18, 1602–1610 (2006)
- 34 E. Ruiz-Hitzky, M. Darder, P. Aranda, “An introduction to Bio-nanohybrid materials: Strategies, Syntheses, Characterization and Applications” Chapter 1, pp 1–40, in *Bio-Inorganic Hybrid Materials*, E. Ruiz-Hitzky, K. Ariga, Y. Lvov, Eds., Wiley-VCH , Weinheim, 2007
- 35 E. Ruiz-Hitzky, M. Darder, P. Aranda, K. Ariga, *Adv. Mater.*, 22, 323–336 (2010)
- 36 E. Ruiz-Hitzky, P. Aranda, M. Darder, F.M. Moreira Martins Fernandes, C.R. Santos Matos, Sp. Patent 200900104 (2009)
- 37 E. Ruiz-Hitzky, P. Aranda, M. Darder, A.C. Santos de Alcântara, Sp. Patent 200930326 (2009)
- 38 E. Ruiz-Hitzky, M. Darder, P. Aranda, M.A. Martín del Burgo, G. del Real, *Adv. Mater.* 21, 4167–4171, (2009)
- 39 B. Wicklein, M. Darder, P. Aranda, E. Ruiz-Hitzky, *Langmuir* 26, 5217–5225 (2010)